The Role of Primary Health care Providers for Diabetic Patients in Jeddah Regarding Routine Care According to the Immune System

By

Talal Saeed Alghamdi*

***Medical Nursing, Jeddah First Health Cluster, Saudi Arabia**

Hani Mohammed Saleh Alghamdi**

****Medical Nursing, Jeddah First Health Cluster, Saudi Arabia**

Alhasan Yahya Asery***

*****Epidemiologist, Jeddah First Health Cluster, Saudi Arabia**

Ahmad Mohammed Alghamdi****

******Medical Nursing, Jeddah First Health Cluster, Saudi Arabia**

Abdulkarim Mohammed Alsabyani*****

*******General Physician, Jeddah First Health Cluster, Saudi Arabia**

Ziyad Sultan Aljohani******

********General Physician, Jeddah First Health Cluster, Saudi Arabia**

Mushari Atiq Alsulami*******

*********Radiology Technologist, Jeddah First Health Cluster, Saudi Arabia**

Abdullah Munif Alrashed********

**********General Physician, Jeddah First Health Cluster, Saudi Arabia**

Fatama Idrees Takarony*********

***********Health Assistant, First Health Cluster, Saudi Arabia**

Abstract: The current study aimed to investigate the role of primary health care providers for diabetic patients in Jeddah in relation to routine care according to the immune system. The study concluded the importance of this role for diabetic patients in the context of routine care follow-up for immune diseases.Keywords: Primary Healthcare - Elderly - Jeddah City - Artificial Intelligence - proposed vision.

Keywords: Primary Health care - Diabetic Patients - Jeddah - Routine Care - Immune System.

I. INTRODUCTION

Diabetes is a major worldwide epidemic with >415 million individuals living with the disease. This number is expected to grow to a staggering 642 million by 2040 (1). According to the American Diabetes Association, diabetes affects 29.1 million Americans, or 9.3% of the population. Diabetes management in the United States presents several challenges: 20% of individuals with diabetes remain undiagnosed, 1.4 million new cases are diagnosed annually, and one-third of adults with diabetes are not at the general recommended A1C goal of <7% (2).

In addition to the clinical burden of diabetes, the financial impact is also substantial. The cost of diagnosed diabetes was ~$245 billion in 2013, representing a 41% increase over the previous 5 years. These costs include inpatient care, prescriptions and supplies for the management of the disease and its complications, doctor office visits, and nursing care and facility stays (3).

According to the Centers for Disease Control and Prevention, primary care visits accounted for 52.3% of all medical office visits in the United States in 2013. Diabetes was the fifth ranked primary diagnosis for such visits, accounting for ~3% of primary diagnoses (4). At the heart of diabetes management is the challenge of adequately controlling glucose over the long term to prevent complications such as retinopathy, nephropathy, and neuropathy while avoiding potentially life-threatening hypoglycemia in the short term.

Antimicrobial resistance (AMR) has been a long-standing issue, gaining prominence with the discovery of penicillin in 1928 [1] and significantly improving human health and life expectancy. AMR has emerged because of antimicrobial misuse and natural selection, requiring a holistic surveillance approach using a One Health approach that considers interactions between humans, animals, and the environment [2]. The impact of AMR on bacterial consortia is greatly influenced by the interactions that occur within them, and these interactions are influenced by the availability of resources [3]. The effects of these interactions, as well as the influence of the ecological context, are frequently ignored when evaluating the efficacy of antimicrobials and the emergence of resistance. AMR is typically viewed as a characteristic specific to individual strains; however, the interactions between and within clinical and environmental microbial communities, as well as the physical properties of these groupings, tend to strongly influence the susceptibility rate of physiological and antimicrobial states of bacteria [4], [5]. The rise in AMR pathogens, characterized by new resistance mechanisms that result in multidrug resistance (MDR) pathogens [6], poses a global threat, with 700,000 annual deaths due to resistant bacteria, a potential increase of 10 million by 2050 [7], [8], and a critical need for new antibiotics for complex procedures and common conditions. This requires the need to take actions to avoid a "post-antibiotic era", in which even simple infections can be fatal [9].

Despite the public health problems AMR poses, the host's immune system is a crucial ally. For an infection caused by any AMR pathogen to succeed, the pathogen must establish itself and replicate within its host. However, the vertebrate immune system acts as the most important barrier against infection. The immune system is an elaborate structure of molecules and cells that work together to respond to infectious agents, toxins, and danger signals [10], [11]. Immune response mechanisms are divided into two types: the innate immune response, which includes reactions aimed at combating pathogenic organisms and environmental threats at the cellular and molecular levels; and acquired immunity, which is activated by recognizing foreign proteins known as antigens. The dynamics of infection and control begin when the pathogen and the host come into contact [10], [11].

In this dynamic context, the gastrointestinal tract plays an important role, as it is a tissue constantly exposed to stress conditions from pathogenic and non-pathogenic bacteria, making it the most immunologically active organ in the body [12].

Accessible alternatives, such as theoretical and mathematical models, are essential for understanding and predicting AMR, and the scientific community has made significant efforts to clarify the fundamental mechanisms of bacterial resistance. Most efforts have focused on modeling individual strains, for example, [13], [14], [15], and recent attention has been paid to modeling microbial consortia [16], [17], [18]. However, to the best of our knowledge, no study has explored the dynamic transitions generated by the immune system or revealed multiple equilibrium points. Therefore, this study fills these gaps by investigating the spread of resistance within microbial communities, particularly emphasizing microbial competition and the influence of the host immune system in combating infections.

The first objective of this study is to explain the dynamics of bacterial resistance when two distinct types of bacteria coexist and compete in the infected host organism. The second objective is to evaluate how the host's immune system influences the spread of bacterial resistance, especially considering the coming era when antibiotic effectiveness is decreasing and emphasizing the critical role of the immune system as the first line of defense. The third objective is to validate our mathematical model using data from *Escherichia coli*, which is a classic example of a colonizing bacterium in the digestive tracts of most vertebrates [19]. To achieve these objectives, we propose a deterministic mathematical model using ordinary differential equations (ODEs) that represents the spread of AMR when two bacterial strains compete. We analyze the existence and stability of equilibrium solutions and explore bifurcations in these equilibria under variations in the parameter representing the rate at which the host's immune system eliminates bacteria. The model and its results are innovative, and we anticipate that they will have a significant impact on the theoretical study of AMR worldwide.

FIGURE 1.

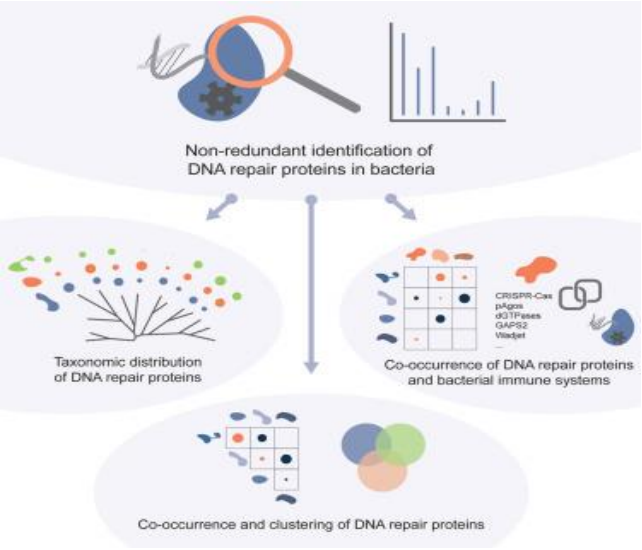

Continuous glucose monitoring (CGM) technology is one advancement that can improve overall glycemic control while minimizing hypoglycemia (5). CGM has been available since the late 1990s. However, its use is not widespread. Clinical inertia is often cited as major barriers to the use of CGM. The introduction of new technology into a clinic requires initiative, awareness of its benefit, and efforts to integrate its use into the routine clinic workflow. This article reviews the use of CGM in the primary care setting and addresses some of the barriers to clinical implementation.

Crucial Role of Primary Care in Diabetes Management:

Primary care has become a center point for diabetes management. A 2014 study by the Endocrine Society demonstrated an increasing demand for, compared to the available supply of, endocrinologists and predicted that there would be a shortage of 2,700 endocrinologists in the United States by 2025 (6). Much of that growing demand is driven by the aging population because the prevalence of type 2 diabetes increases with age. A 2012 study using the National Provider Identifier Registry showed that the ratio of endocrinologists to adults ≥65 years of age was ~6,194 to 1, and the average wait time to visit such a specialist was 3–4 months (7). Currently, primary care providers (PCPs) deliver clinical care to ~90% of individuals with type 2 diabetes, and this proportion is likely to increase over time (8).

With a burgeoning diabetes population, the judicious use of time by PCPs is crucial in successfully managing patients. The challenge is that diabetes management has become increasingly complex as a result of multiple medication categories (including combination medicines), the need to avoid hyper- and hypoglycemia, multiple choices of medical devices for managing diabetes, the need to facilitate patients' lifestyle changes, and other issues. In a study of trends in the complexity of diabetes care in the primary care setting between 1991 and 2000, the number of individuals with diabetes taking at least five medications increased from 18.2 to almost 30%. Despite this ever-increasing complexity, the proportion of medical visits lasting >20 minutes increased only 3.1% during this same time period (9).

FIGURE 2.

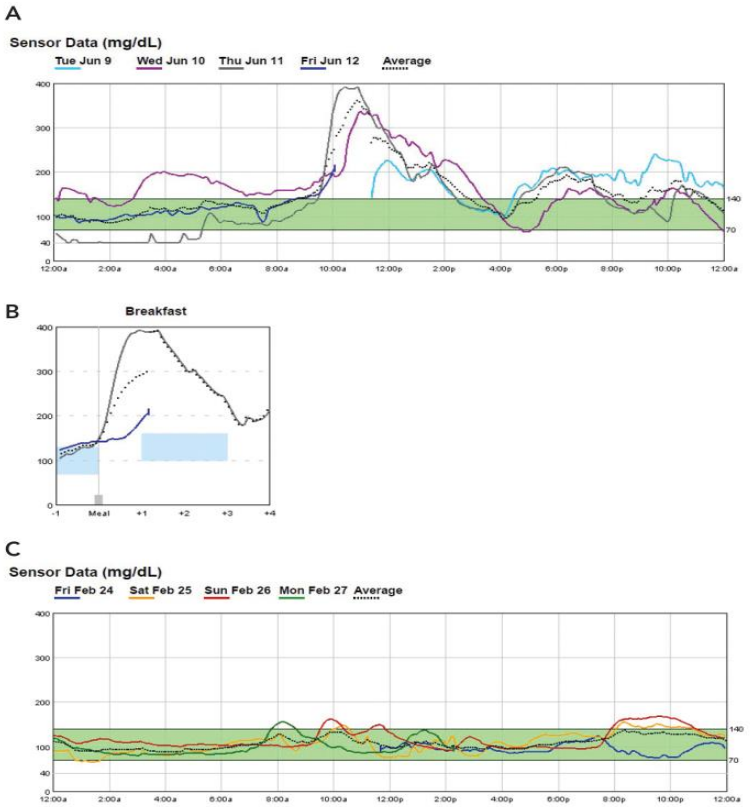

Patients who agree to enter the program receive a complete instruction sheet, provide informed consent, and have a sensor inserted. Patients are typically sent home with a glucose meter to calibrate the sensor and supplies (i.e., extra tape and wipes) for maintaining sensor wear. Patients typically wear the sensor for up to 6–7 days, but meaningful data may be obtained in the 72-hour window required to bill under Current Procedural Terminology (CPT) code 95250 (see billing discussion below).

At the end of the evaluation period, patients return to the clinic, where their sensor data are uploaded and all glucose readings, food, medication, and activity logs are entered into the P-CGM software (or synchronized, if they used a logging app). The HCP notes any trends and habits that may be affecting glucose control and medication regimens.

In some cases, when a diabetes educator is the primary data reviewer, he or she will discuss observations in the reports and areas for improvement, including medication management or lifestyle modifications, with the PCP. Once an appropriate plan is created between the educator and provider, the reports are reviewed in detail with the patient, explaining salient points and discussing suggested modifications. Receiving patient feedback on the plan is important to ensure adherence.

In some health care systems, P-CGM is a service that is facilitated mainly by the diabetes educator, who does initial patient education, handles data entry, and meets with patients to review results. In other cases, P-CGM may be handled by a registered nurse, medical assistant, or physician's assistant. Limiting the number of people who are involved keeps the process consistent and limits the chance of errors that could negate the entire P-CGM study.

n bacteria, genomic DNA can be damaged by both endogenous and exogenous processes. Endogenous processes include stalled replication forks, metabolic/radical products, and nucleases,[1,2,3] whereas exogenous processes include UV radiation and other DNA-damaging agents, including antibiotics, chemicals, and acids.[1,4,5] As genomic DNA encodes essential genes, maintaining its integrity is vital. To this end, bacteria encode diverse DNA repair pathways.[6,7,8] Mutations of single DNA nucleotides are generally repaired by base excision repair, nucleotide excision repair, or mismatch repair pathways.[9,10] In contrast, double-stranded DNA breaks (DSBs) and other DNA lesions are generally repaired by either non-homologous end joining (NHEJ) or homologous recombination (HR) pathways.[7,11] Alternatively, DSBs can be repaired through microhomology-mediated end joining (MMEJ)[12] and single-strand annealing (SSA)[13] pathways, of which proteins involved partially overlap with NHEJ or HR pathways. NHEJ involves the removal of damaged bases, error-prone resynthesis, and direct ligation of the free DNA ends.[14,15] While NHEJ is the main mode of DSB repair in eukaryotes, only 22% of bacteria encode homologs of known NHEJ proteins.[16,17] Instead, DSBs are mostly repaired through HR pathways in bacteria.[11,18] During HR, a DNA template homologous to the damaged DNA is used to repair the DSB, which allows mutation-free DNA repair.[18,19] As most bacteria harbor multiple copies of their genome (or duplicated genomes are present during replication), homologous DNA templates required for HR are generally readily present in bacteria.[20]

Distinct bacterial HR pathways exist, each of which involve proteins that can also be used in other distinct DNA repair pathways.[18] Most bacterial HR pathways involve the protein RecA (i.e., RecA-dependent HR pathways). While RecA-independent HR pathways also exist, their activity has only been observed under specific circumstances (e.g., in bacteria without RecA, at [short/inverted] direct repeats and for specific types of DNA damage)[13,21,22,23] and are therefore not discussed further here. RecA-dependent HR pathways rely on the formation of a single-stranded (ss)DNA fragment to which RecA binds. Consequentially, ssDNA-bound RecA forms a presynaptic filament that places the ssDNA in a helical B-form conformation, which allows the ssDNA to invade homologous dsDNA sequences.[24,25,26] This facilitates strand exchange, after which HR can be completed through branch migration and resolving the Holliday junction by various proteins (e.g., RecG, RecQ, Rus, and/or RuvABC[27,28,29]). Preceding strand invasion, RecA relies on one of various DNA repair pathways for the formation of and/or RecA loading onto ssDNA fragments. Well-studied bacterial DNA repair pathways involved in ssDNA generation and RecA loading include Rec(F)OR, RecBCD, AddAB, and AdnAB (Figure 3).

FIGURE 3.

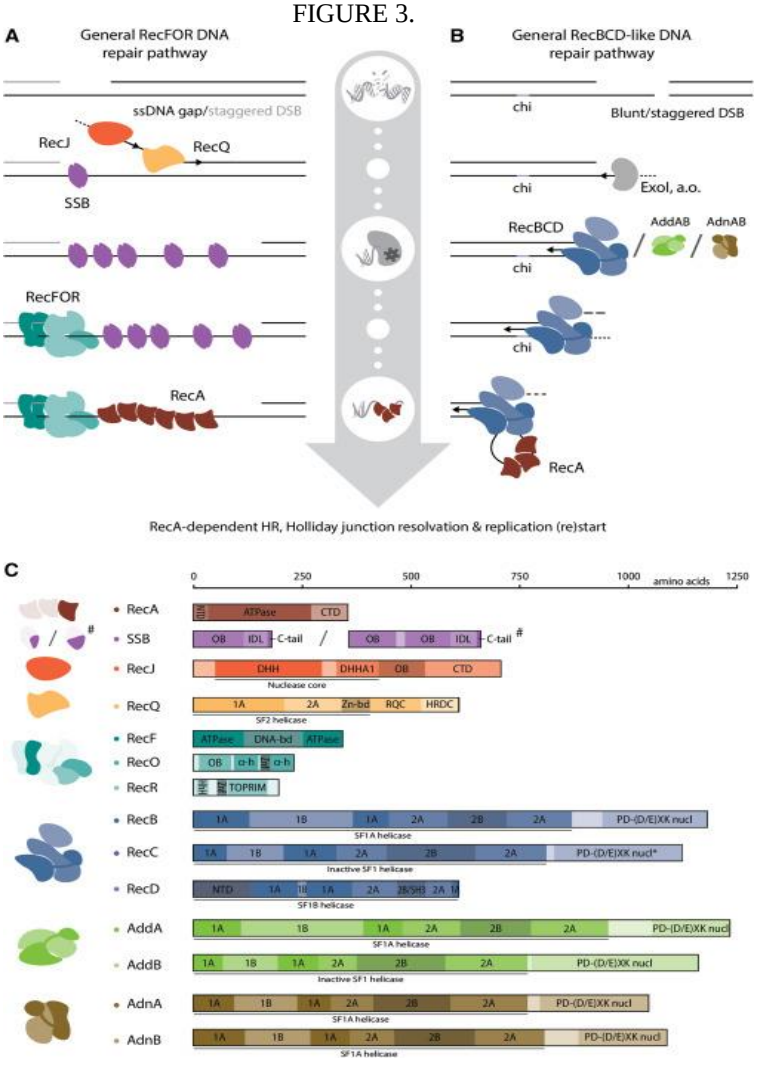

Figure 1. Start of homologous recombination pathways in bacteria and domain architecture of proteins involved

(A) The general RecFOR repair pathway as described for *T. thermophilus*, *D. radiodurans*, and *E. coli*. RecQ helicase and RecJ nuclease widen the ssDNA gap or ssDNA overhang at a ssDNA gap or DSB, respectively. SSB binds exposed ssDNA. The RecFOR complex binds ssDNA-dsDNA junctions, or RecOR binds SSB-coated ssDNA, and replaces SSB with RecA.
(B) The general RecBCD-like pathway as described for *E. coli*. Blunt-ended DSBs are processed by nucleases like ExoI to form blunt-ended DSBs. The RecBCD complex (or AddAB in *B. subtilis* or AdnAB in *M. smegmatis*) assembles on the blunt-ended DSB and processes the dsDNA by unwinding and cleavage of ssDNA. Once a chi site is bound, cleavage of the chi-site-containing strand is inhibited, after which that strand is looped out, and RecA is loaded onto it. In Rec(F)OR, RecBCD, AddAB, and AdnAB pathways, RecA-loaded ssDNA forms a synaptic filament that can invade a dsDNA template. Upon base pairing between complementary strands, a (double) Holliday junction is formed. RuvABC resolves the Holliday junction, after which DNA polymerase fills in the ssDNA gaps.

(C) Domain architecture of proteins that initiate homologous recombination in bacteria. NTD, N-terminal domain; CTD, C-terminal domain; OB fold, oligonucleotide-binding fold; IDL, intrinsically disordered linker; C-tail, C-terminal tail; DHHA1, DHH associated 1; 1A/2A, RecA-like domains 1/2; 1B/2B, domains inserted in RecA-like domains 1A/2A; SF1A/SF1B/SF2 helicase, superfamily 1/2 A/B helicases; Zn-bd, zinc-binding domain; RQC, RecQ C-terminal domain; HRDC, helicase and RNaseD C-terminal domain; DNA-bd, DNA binding domain; α-h, α helical domain; Znf, zinc finger; HhH, helix-hairpin-helix domain; TOPRIM, topoisomerase-primase domain; PD-(D/E)XK nucl, nuclease domain with conserved catalytic motif PD-(D/E)XK; SH3, SRC homology domain 3. *, catalytically inactive. #In most bacterial clades, SSB contains one OB fold and forms a homotetramer, whereas in the Deinococcota, SSB contains two OB folds and forms homodimers.[30] See also Figure S1 for catalytic residues and motifs of archetype proteins.

The RecFOR pathway is typified by RecF, RecO, and RecR (Figure 1A).[31,32,33,34,35] The RecFOR pathway is involved in the repair of ssDNA gaps that can occur during DNA replication[31] and in plasmid recombination and conjugation.[35] Such ssDNA gaps are sometimes extended by the nuclease RecJ, in cooperation with the helicase RecQ,[36,37] after which the ssDNA is coated by ssDNA-binding protein (SSB).[35,37] After the DNA replication machinery stalls at these ssDNA gaps, the RecFOR complex assembles on the dsDNA/ssDNA transition[38,39]: a RecF dimer assembles on the dsDNA, a tetrameric RecR ring clamps the ssDNA, and RecO binds ssDNA on the RecF-distal side of the RecR ring.[33,37] In the absence of RecF, a RecOR complex can also assemble in the middle of an ssDNA gap or on a staggered DSB *in vitro*, where the RecF dimer is replaced by an additional RecO monomer.[40] The bound Rec(F)OR complex interacts with SSB and stimulates loading of RecA onto SSB-coated ssDNA.[41] Beyond repairing ssDNA gaps, the RecFOR pathway also repairs DSBs when more efficient DSB repair pathways are absent.[36] In that case, RecQ and/or RecJ process blunt or staggered DSBs to generate stretches of ssDNA.[36,37]

The RecBCD pathway is typified by the RecBCD helicase-nuclease complex (Figure 1B). RecBCD binds blunt-end DSBs, which can be generated from staggered-end DSBs by nucleases such as RecJ, SbcCD, and ExoI.[7] The dsDNA is pulled through RecBCD by the helicase domains of RecB and RecD, while the RecB nuclease domain asymmetrically cleaves both unwound DNA strands that exit the RecBCD complex.[42,43] RecBCD-mediated dsDNA degradation continues until RecC binds a chi (crossover hotspot instigator) site, a short sequence motif found in the genome. Chi site binding changes the activity of RecBCD: while degradation of the 5′ end DNA strand is enhanced, degradation of the 3′ end is attenuated, and the formed 3′ ssDNA strand is bulged out of the RecBCD complex.[44,45] RecA is loaded onto this 3′ ssDNA,[44] after which strand exchange takes place, and DNA repair is completed. It has recently been suggested that RecBCD also functions in ssDNA gap repair, blurring the lines between distinct DNA repair pathways.[46]

The AddAB pathway is typified by the AddAB helicase-nuclease complex (Figure 1C).[42] Akin to RecBCD, the AddAB complex recognizes and processes blunt-end DSBs, recognizes a (distinct) chi site, and generates a 3′ ssDNA strand onto which RecA is loaded.[47,48] Although the proteins that comprise the RecBCD and AddAB complexes are homologous and function in a similar fashion, major differences between the complexes exist (Figure 1C): RecBCD consists of three subunits (RecB, RecC, and RecD), in which RecB is a helicase-nuclease, RecC is a helicase-nuclease of which both domains are inactive, and RecD is a helicase (and lacks a nuclease domain).[44] In contrast, AddAB consists of two subunits only (AddA and AddB), each of which contains a helicase domain (inactive in AddB) and an active nuclease domain.[48] Furthermore, RecBCD unwinds the DNA strands at a different rate (causing ssDNA loop formation in front of the complex), while AddAB translocates both DNA strands at the same rate and therefore requires SSB to prevent cleavage product reannealing.[42,45,47,49] The AdnAB repair complex is closely homologous to AddAB.[50] However, in contrast to AddAB, in AdnAB, both subunits (AdnA and AdnB) contain functional helicase and nuclease domains.[42] Akin to RecBCD, AdnAB does not require SSB for processive strand unwinding, but no chi site has been identified.[51,52,53,54]

Beyond DNA repair, RecBCD and AddAB have also been implicated in prokaryotic immunity.[44,55,56,57,58,59,60,61,62,63,64] RecBCD can directly degrade phage linear dsDNA genomes or replication intermediates that have exposed dsDNA ends.[55,56] As such, phages have developed various inhibitors to counteract RecBCD activity.[65,66,67,68] Furthermore, the products of RecBCD- and/or AddAB-mediated invader DNA degradation result in the formation of DNA degradation products that indirectly or directly guide other prokaryotic immune systems, including CRISPR-Cas systems[57,58,59] and prokaryotic Argonaute (pAgo) proteins.[60,61,62,63,64] This suggests that these immune systems rely on DNA repair complexes, that they act in conjunction, or that synergistic effects between these DNA repair complexes and immune systems exist. As such, analyses of the co-occurrence of DNA repair proteins and these and other prokaryotic immune systems might shed light on their functional co-dependence and the mechanisms underlying prokaryotic immunity. However, the high degree of homology between DNA repair proteins or domains thereof (Figure 1C) makes the accurate identification of DNA repair proteins challenging. While previous studies have shed light on the distribution of proteins involved in HR,[69,70,71,72,73] we found that available TIGR/HMM profiles do not accurately distinguish different DNA repair enzymes, hindering subsequent analyses.

Here, we describe a unique search strategy to identify and classify bacterial DNA repair proteins, involving new HMM profiles with query sequences from diverse phyla, followed by reverse HMM score-based filtering. We used this stringent search strategy to identify DNA repair proteins in the RefSeq database, which facilitated accurate analyses of their taxonomic distribution, (co-)occurrence, and genomic clustering over the bacterial phyla. Furthermore, by identifying prokaryotic immune systems using DefenseFinder and analyzing their co-occurrence with DNA repair proteins, we confirm existing associations with CRISPR-Cas systems and find many novel correlations including pAgos, dGTPases, GAPS2, and Wadjet.

As such, this work provides an updated view on the distribution of DNA repair proteins in bacteria, extends our insights into their genomic clustering, and sheds light on the co-occurrence between DNA repair proteins and prokaryotic immune systems.

Results:

Accurate identification and classification of DNA repair proteins:

To perform phylogenetic and taxonomic distribution analyses of DNA repair proteins, accurate identification and classification are required. In earlier studies, several HMM profiles have been developed to identify the homologs that belong to specific protein families.[70,71,74] Using these publicly available HMM profiles, we attempted to identify DNA repair proteins in the representative scaffold and whole genomes of the RefSeq database (accessed on January 16, 2021, 7,249 genomes). However, the presence of certain DNA repair proteins appeared highly overestimated (e.g., 27,589 RecB hits for TIGR00609, >3 copies per genome; Table S1). Furthermore, multiple proteins were identified by multiple individual HMM profiles. This indicates that search constraints are too lenient for accurate identification and classification, probably due to the high degree of homology and similar domain architecture of distinct DNA repair proteins (Figure 1C). To generate new HMM profiles enabling more accurate identification, for each DNA repair protein, we selected ≥10 sequences (11–17) from highly different phylogenetic groups (Figure 2A). However, HMM searches using the newly constructed HMM profiles still resulted in the overrepresentation of various proteins (e.g., 27,846 hits for RecB, >3 copies per genome; Figure 2B), and >20,000 proteins were identified by multiple HMM profiles (e.g., 90,698 proteins were identified as RecB, RecD, AddA, AddB, AdnA, and AdnB; Figure S2A). This underscores the challenge of classifying highly homologous DNA repair proteins. These results imply that further filtering is required to facilitate accurate identification of DNA repair proteins.

FIGURE 4.

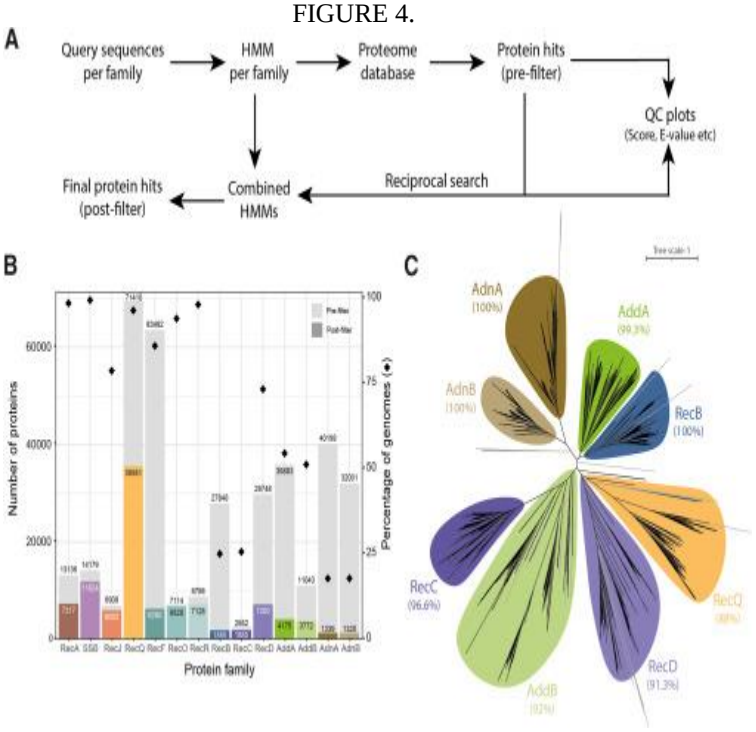

Figure 4. Accurate identification of DNA repair proteins and phylogenetic validation of helicases

(A) Schematic representation of the pipeline used for DNA repair protein identification and classification. 11–17 sequences per protein family were selected from diverse bacterial phyla to construct HMM profiles. These profiles were used to search the proteomes from 7,249 RefSeq genomes. The obtained (overlapping; pre-filter) hits were subjected to a reciprocal search using our collection of HMM profiles, after which proteins were classified using the highest scoring HMM profile (post-filter).
(B) Number of proteins identified per protein family pre-filter (gray) and post-filter (colored, primary y axis). Diamonds (◆, secondary y axis) indicate the percentage of genomes that contain the corresponding protein (post-filter).
(C) Unrooted phylogenetic tree of the SF1 and SF2 helicase domains of DNA repair proteins RecQ, RecB, RecC, RecD, AddA, AddB, AdnA, and AdnB. Clades are labeled and colored according to the protein classifying this clade, and the percentages indicate the proteins correctly classified in this clade. Proteins with classifications that do not follow the phylogeny are colored gray. See also Figure S2 for proteins identified by multiple HMM profiles and Figure S3 for a midpoint-rooted tree with protein annotations and corresponding HMM scores.

To obtain accurate classification of the DNA repair proteins, for each protein identified, reciprocal HMM searches were performed using the new HMM profiles developed (Figure 2A).

Using the reciprocal search strategy, query proteins were first identified using the different HMM search profiles (i.e., for each type of DNA repair protein, an HMM profile exists, and each of these profiles is used to identify a pool of DNA repair proteins). Subsequently, for each identified DNA repair protein, an HMM score was generated for each of the HMM search profiles (i.e., for each type of DNA repair protein). After that, for each DNA repair protein, the different HMM scores were ranked, and the protein was assigned the identification of the HMM search profile that generated the highest HMM score.

The reciprocal HMM searches facilitated a classification of DNA repair proteins for which no overlapping classification exists (Figures 2B and S2B). RecA and SSB are present in ~99% of the genomes (Figure 2B). These findings underscore the central role of these SSBs in different DNA repair pathways.[26,37,42] Similarly, RecJ and RecQ are present in 79% and 97% of genomes, respectively (Figure 2B). The proteins RecO and RecR are identified in >94% of all genomes, whereas RecF is identified in 86% of all genomes (Figure 2B). In line with the *in vitro* activity of RecOR without RecF,[75] this implies that RecF is not essential in Rec(F)OR pathways. RecB and RecC are found in 25%–26% of all bacterial genomes, while RecD is found in 73% (Figure 2B). This confirms previous analyses that most RecD proteins have a function outside the context of RecBCD.[76,77] Finally, AddA and AddB are found in 55% and 51% of genomes, whereas AdnA and AdnB are present in 18% of genomes (Figure 2B).

To verify the classification and obtain insights about the shared ancestry of DNA repair proteins, we performed phylogenetic analysis of the SF1 helicase domain-containing DNA repair proteins (RecB, RecC, RecD, AddA, AddB, AdnA, AdnB) and SF2 helicase RecQ (Figure 1C). 96.3% of proteins cluster in distinct phylogenetic clades according to their classification, which endorses the accuracy of our method (Figures 2C and S3). The small fraction of proteins for which the assigned classification does not match the phylogeny generally have a low score for all reverse HMM searches and form (sub)clades with long branch lengths, which indicates they represent distantly related proteins (Figures 2C and S3). While increasing the cutoff score could limit these inaccurate identifications, it would also lower the number of correctly identified proteins. The phylogeny reveals that the AddA-RecB, AddB-RecC, and AdnA-AdnB pairs have common ancestors (Figure 2C),[41] in contrast to an earlier study in which it was suggested that AddAB and RecBCD proteins evolved from AdnAB proteins.[78] RecD and RecQ form individual clades, and within the RecQ clade, there is a clear distinction of two subclades (Figure 2C). The current identification and classification strategy allows for further analysis of the distribution of these DNA repair proteins in bacteria.

Global taxonomic distribution of DNA repair proteins:

To obtain a clear image of the taxonomic distribution of DNA repair proteins across the bacterial phyla, we analyzed the abundance of DNA repair proteins in the different bacterial phyla (Figure 3). We limited our analysis to phyla with ≥6 representative genomes in the representative scaffold and whole genomes of the RefSeq database and pooled the remaining genomes as "other." In accordance with their high abundance, RecA, SSB, and RecQ are present in all bacterial phyla (Figure 3; Table S2). All three RecFOR proteins are present in most bacterial clades (Figure 3), while Acidobacteriota, Aquificota, Mycoplasmatota, Nitrospirota, Planctomycetota, and Thermodesulfobacteriota mostly encode only RecOR and lack RecF. RecFOR proteins are almost completely absent in Thermotogota (which form a separate clade between Gracilicutes and Terrabacteria[79,80]). Given that Thermotogota undergo extensive DNA exchange[81,82] and that certain Thermotogota species are naturally competent,[83] a more divergent Rec(F)OR pathway or another analogous DNA repair system might exist in Thermotogota.

FIGURE 5.

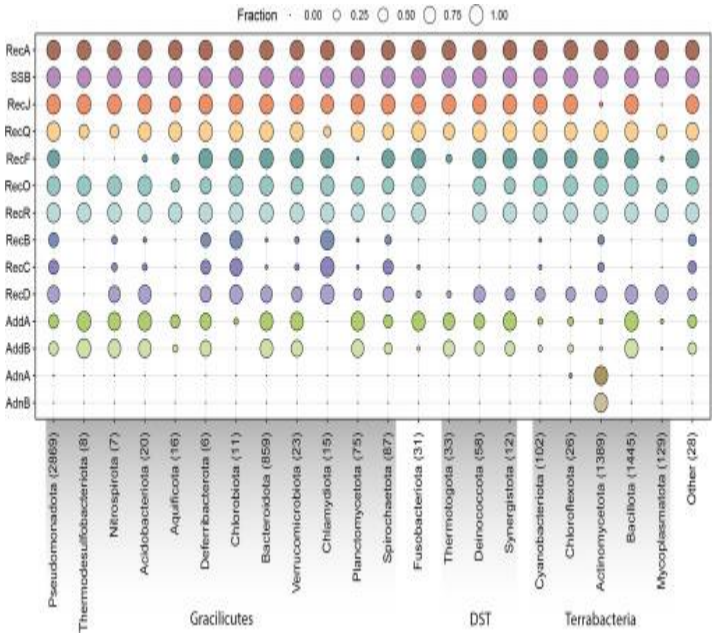

Figure 5. Taxonomic distribution of DNA repair proteins

Bubble plot indicating the fraction of genomes that encode specific DNA repair proteins per bacterial phyla (ordered according to bacterial phylogeny[79,80]). Phyla with <6 genomes were grouped as "other."[79,80] Numbers next to the phyla names indicate the number of genomes present in the total dataset of 7,249 genomes.

Despite RecBCD being arguably the most-studied bacterial HR complex,[42,43,44,45,68,84] RecB and RecC are (almost) completely absent in 12 out of 21 phyla included in our analysis, including bacteria belonging to the Terrabacteria and DST (Deinococcota, Synergistota, and Thermotogota) groups. RecBCD is present in >50% of bacteria that belong to the Gracilicute group Chlamydiota, Chlorobiota, Deferribacterota, and Pseudomonadota phyla (Figure 3; Table S2). In the remaining five Gracilicute phyla, RecB and RecC are present in ≤20% of genomes. Several bacterial phyla that do not encode RecBC do encode RecD (e.g., Bacillota, Chloroflexota, Deinococcota, and Mycoplasmatota), which indicates the existence of the RecD variant "RecD2," as previously indicated[76,77] (Figure 3).

In general, AddAB is (sometimes sparsely) distributed over all phyla except Chlamydiota, and AddA is slightly more widespread than AddB (Figure 3). In line with previous literature, AdnA and AdnB are 99.96% specific to Actinomycetota.[71] Various phyla, including the Terrabacteria clades Chloroflexota, Cyanobacteriota, and Mycoplasmatota, encode (almost) no RecBC, AddAB, and/or AndAB complexes. RecJ is found ubiquitously in all phyla except Actinomycetota and Mycoplasmatota, which do encode RecOR (Mycoplasmatota) or RecFOR and AdnAB (in Actinomycetota) (Figure 3). This implies that HR occurs independently of RecJ in these phyla or that they encode more divergent RecJ homologs or analogous proteins with a similar function. Combined, our analysis reveals phyla-specific patterns of DNA repair proteins, of which certain findings invite further exploration.

Co-occurrence and co-encoding of DNA repair proteins:

Rec(F)OR, RecBCD, AddAB, and AdnAB form complexes in certain bacterial species.[37,42,43,47,51] Principal-components analysis (PCA) confirms that proteins of the DNA repair complexes RecFOR, RecBC, AddAB, and AdnAB are distributed accordingly (Figure 4A). To understand if co-occurrence (or exclusion) also exists between these and other DNA repair proteins, the co-occurrence of all DNA repair proteins was investigated (Figures 4B and 4C). The presence of Rec(F)OR-coding genes is strongly correlated, with representation of all three proteins in 83% of the genomes, while 11% of the genomes encode RecOR but not RecF (Figures 4B and 4C). Also, the presence of AdnA/AdnB, AddA/AddB, and RecB/RecC protein combinations is strongly correlated (Figure 4B). As RecD is often encoded in genomes independently of RecBC (in 65% of the genomes), it does not cluster with RecBC in the PCA (Figure 4A), and the correlation for RecD co-occurrence with RecBC is weak (Figure 4B). However, RecBC is rarely found in the absence of RecD (Figure 4C).

FIGURE 6.

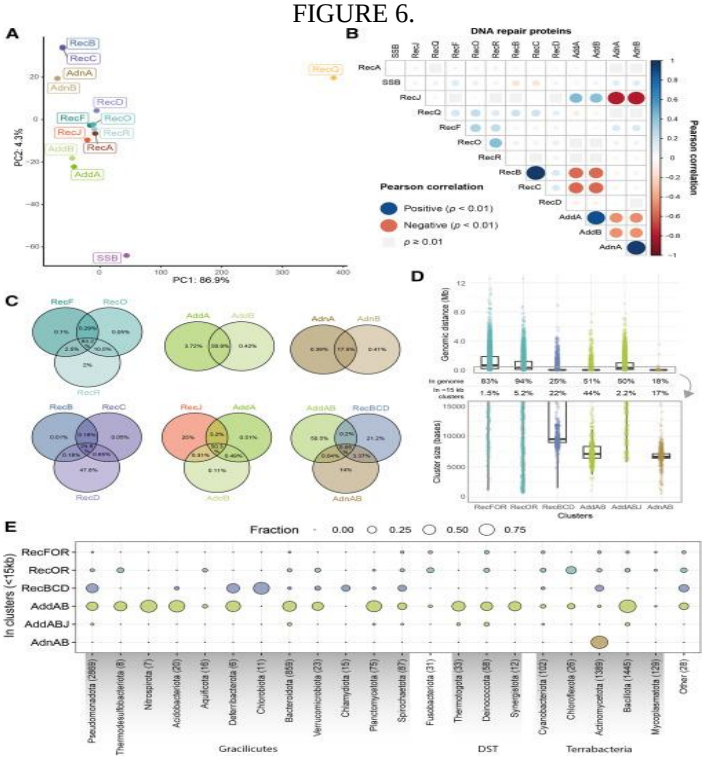

Figure 6. Co-occurrence and genomic clustering of DNA repair proteins

(A) PCA plot indicating similarity in the distribution of DNA repair proteins across 7,249 bacterial genomes with two most-important PCs (PC1: 86.9% and PC2: 4.3%). Proteins close together indicate a similar overall distribution of these proteins.

(B) Pairwise Pearson correlation of the presence of each DNA repair protein across 7,249 bacterial genomes. Red/blue circles represent negative/positive correlations, with size and color intensity indicating correlation strength. Gray squares indicate insignificant correlations ($p \geq 0.01$).

(C) Venn diagrams indicating the percentage of genomes having co-occurrence of DNA repair proteins for RecFOR, RecBCD, AddAB (with and without RecJ), and AdnAB. In addition, a Venn diagram indicating the co-occurrence of complete AddAB, RecBCD, and AdnAB genomic clusters is shown. Percentages indicate the genomes with the specified proteins compared to the total number of genomes (7,249) considered.

(D) Genomic distance between genes encoding co-occurring DNA repair proteins. If three genes are considered (RecFOR, RecBCD, AddABJ), then the maximum distance is shown. Genes are considered clustered when the maximum distance is <15 kb (see bottom). See also Figure S4 for each combination and individual cluster sizes.

(E) Taxonomic distribution of DNA repair protein clusters <15 kb in bacterial phyla (ordered according to bacterial phylogeny[79,80]). Numbers next to the phyla names indicate the number of genomes present in the total dataset of 7,249 genomes. Phyla with less than 6 genomes are grouped as "other."

The presence of AddAB is negatively correlated with both of the other DSB repair complexes, RecBC(D) and AdnAB (Figures 4B and 4C), which suggests that they are mutually exclusive. As expected due to their high abundance, proteins that occur in >90% of genomes (SSB, RecA, RecR, RecQ, RecO) mostly show weak correlations with other proteins (Figure 4B). However, the presence of RecQ is positively correlated with the presence of RecFOR and RecBCD proteins, while a slightly negative correlation is observed for the presence of RecQ and AddAB proteins (Figure 4B). While a functional link exists between RecQ and RecFOR (Figure 1A), to our knowledge, no such links have been established between RecQ and RecBCD. The negative correlation of RecQ with AddAB could be attributed to the complementary roles of RecQ and RecJ in processing DSBs (followed by the RecFOR pathway)[36,85]; the presence of RecJ is positively correlated with AddAB (Figure 4B), which suggests that AddAB and RecJ function in conjunction. Combined, these results confirm the co-occurrence of known DNA repair proteins (Rec(F)OR, RecBCD, AddAB, and AdnAB) and reveal co-occurrence patterns that have not been identified before.

In bacteria, genes encoding proteins that function in conjunction sometimes cluster in the genome, for example in operons.[86] To determine if the genomic clustering of genes encoding DNA repair proteins is conserved, we analyzed the genomic distance between the genes encoding complex-forming DNA repair proteins (Figure 4D). Despite their linked functionality and omnipresence, Rec(F)OR-coding genes rarely cluster (Figures 4D and S4), as described previously.[69] In contrast, 90% of RecBCD-coding genes are found in clusters, mostly in Pseudomonadota, Deferribacterota, and Chlorobiota (Figures 4D and 4E). In contrast, in Chlamydiota, RecBCD-coding genes are present in all studied genomes (Figure 3) but rarely clustered (Figure 4D). AddA- and AddB-coding genes cluster in 87% of AddAB-encoding genomes (Figure 4D) distributed across most phyla (Figure 4E), whereas RecJ, the occurrence of which is strongly positively correlated with AddAB (Figure 4B), is rarely encoded in proximity to AddA or AddB (Figure 4D). The Actinomycetota AdnAB pair exists in clusters in 97% of the AdnAB-encoding genomes (Figures 4D and 4E). Together, these results signify that repair proteins involved in a complex or functional in the same pathway are found in a cluster or putative operon (AddAB, AdnAB, and RecBCD) or are encoded independently (Rec(F)OR).

DNA repair proteins and genome size:

Bacterial genomes widely vary in genome size, with bacteria from certain phyla having smaller genomes than the others (Figure S5). There is a strict correlation between genome size and proteome size (Pearson correlation coefficient [R] = 0.99; Figure 5A), and it has previously been established that a positive correlation also exists between genome size and the number of prokaryotic immune systems encoded.[87,88] To determine if a correlation exists between genome size and the number of DNA repair proteins encoded, we compared the genome size to the total number of DNA repair proteins.

While the number of DNA repair proteins encoded increases up to a genome size of ~5 Mb, it plateaus at ~15–16 DNA repair proteins encoded in larger genomes (Figure 5B). RecQ is diverse and overrepresented in our dataset (with 35,581 copies identified in 6,998 genomes, >5 copies per genome; Figures 2B and 2C). Therefore, we hypothesized that removing RecQ from the analysis would clarify the analysis. When RecQ is excluded, the number of DNA repair proteins plateaus at 9–10 in genomes of ~2.5 Mb and larger (Figure 5B). Pearson correlation analysis confirms that a positive correlation between genome size and DNA repair system abundance exists in genomes <2.5 Mb (R = 0.56) but that this correlation is lost in genomes >2.5 Mb (R = 0.069). This suggests that larger genomes do not necessarily require a larger set of canonical DNA repair proteins to maintain genome integrity.

FIGURE 7.

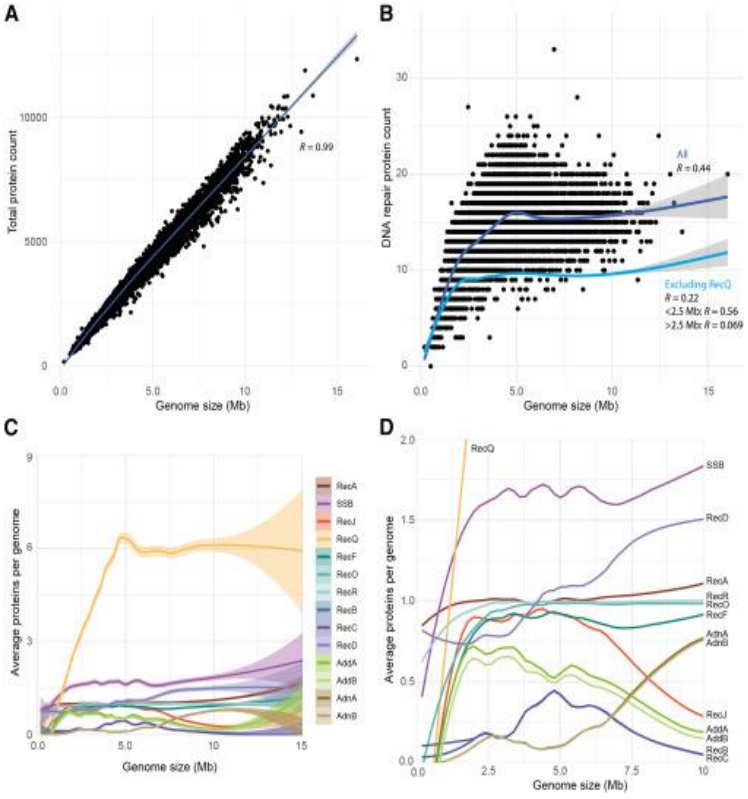

Figure 7. DNA repair proteins and genome size

(A) The total number of proteins in a genome in relation to genome size. The line indicates the average with a 95% confidence interval (shaded). Pearson correlation coefficient R = 0.99.

(B) The total number of DNA repair proteins in a genome in relation to genome size. The dark blue line indicates the average with 95% confidence interval (shaded) and R = 0.44. The light blue line indicates the average of all proteins excluding RecQ. Pearson correlation calculated for all genome sizes, R = 0.22; for genomes <2.5 Mb, R = 0.56; and for genomes >2.5 Mb, R = 0.069.

(C) The number of individual DNA repair proteins in a genome in relation to genome size. The lines indicate averages with 95% confidence intervals (shaded) of individual DNA repair proteins.
(D) Close-up of (C) but excluding confidence intervals. See also Figure S5 for the distribution of genome sizes per bacterial phylum.
Next, we analyzed whether specific DNA repair proteins are more abundant in genomes within a specific genome size range (Figures 5C and 5D). Whereas genomes <1 Mb encode RecA, SSB, and RecR, the other DNA repair proteins only sporadically occur in these small genomes (Figures 5C and 5D). Furthermore, AddAB is most abundant in genomes that are ~1.5–3.5 Mb, whereas RecBCD is most abundant in genomes that are ~3.5–6.5 Mb in size (Figure 5D). In line with Actinomycetota having relatively large genomes (Figure S5), AdnAB is most often found in genomes >5 Mb. This suggests that specific proteins (RecA, SSB, and RecR) are essential and selected for even in small genomes, while DSB repair complexes become more important in genomes with a size beyond 1 Mb (Figure 5D). Furthermore, while the few genomes encoding multiple DSB repair complexes (RecBCD, AddAB, and AdnAB) are large genomes (Figure S5; Table S2), larger genomes do not necessarily encode multiple DNA repair complexes, possibly because their activities would compete with each other.

Co-occurrence of DNA repair proteins and prokaryotic immune systems:

Various prokaryotic immune systems, which protect prokaryotes against mobile genetic elements, including phages and plasmids, function in conjunction with DNA repair proteins.[57,58,59,63,65,89,90] This includes retron Ec48, which senses (phage-mediated) RecBCD inhibition and triggers abortive infection,[65] and type I-E, I-F, II-A, and III-A CRISPR-Cas systems, whose spacer acquisition is enhanced by RecBCD or AddAB.[57,58,59,89] In addition to CRISPR-Cas, the products of RecBCD- or AddAB-mediated dsDNA degradation products are used by pAgo systems as small ssDNA guides.[62,63]
If CRISPR-Cas and pAgo systems, and possibly other immune systems, indeed function in conjunction with DNA repair proteins, then this suggests that correlations between their occurrences could exist. Indeed, previous bioinformatics analyses confirm that the presence of certain CRISPR-Cas subtypes correlates with DNA repair proteins.[71] While such analyses might also expose putative functional relations between other immune systems and DNA repair proteins, such analyses have not yet been extended to other prokaryotic immune systems. Here, we use our classification of DNA repair proteins to investigate their co-occurrences with immune systems as identified by DefenseFinder in whole-genome species representatives in the RefSeq database (>2,300 genomes; Figure 6A).[91]

FIGURE 8.

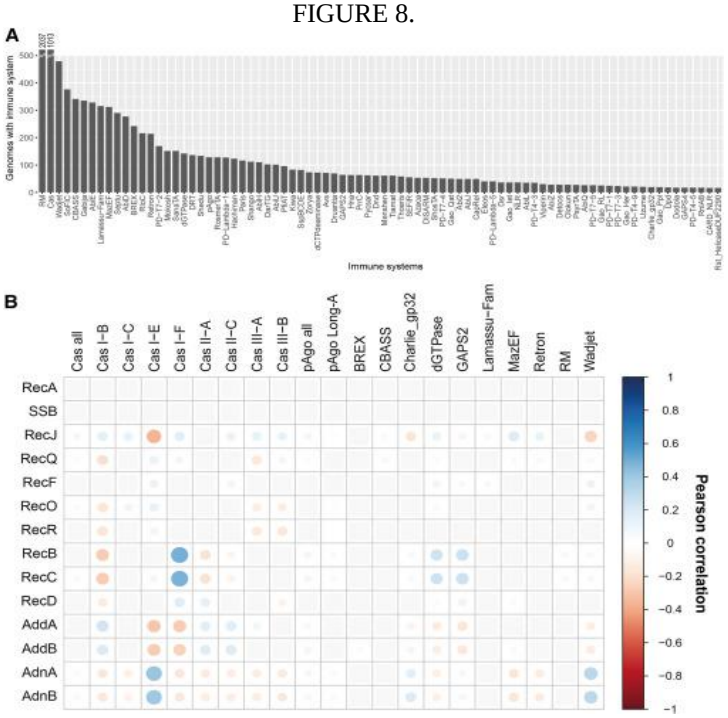

Figure 8. Co-occurrence of DNA repair proteins and bacterial immune systems

(A) Immune systems identified in our dataset using DefenseFinder.[87,91] Systems identified in <15 genomes are not shown.
(B) Pairwise Pearson correlations for selected co-occurring DNA repair proteins and immune systems. Red/blue circles represent negative/positive correlations, with size and color intensity indicating correlation strength. Gray squares indicate insignificant correlations ($p \geq 0.01$). For absolute co-occurrences and more correlations, see also Data S1A (CRISPR-Cas subtypes), Data S1B (pAgo subtypes), and Data S1C (all immune systems). For a full list showing what genomes contain which DNA repair proteins and immune systems, see Table S3.
For the co-occurrence of DNA repair proteins and CRISPR-Cas systems, several positive correlations ($R > 0.3$, $p < 0.001$) can be observed (Figure 6B; Data S1A). The presence of type I-E CRISPR-Cas systems is positively correlated with AdnAB ($R > 0.41$) and negatively correlated with the presence of AddAB ($R < -0.25$) and RecJ ($R = 0.36$; Figure 6B). This suggests that although RecBCD and RecJ play a role in naive and primed spacer acquisition in the *E. coli* type I-E CRISPR-Cas system,[57,89] this is not necessarily the case in other bacteria (Figure 6B; Data S1A). We hypothesize that in bacteria lacking RecBCD and/or RecJ, other nucleases contribute to spacer acquisition, for example ExoVII or AdnAB. In contrast to *E. coli* RecBCD, chi site recognition has not been shown for AdnAB, which suggests that it is not essential for CRISPR adaptation.[57,89,92] The presence of type I-F CRISPR-Cas systems is positively correlated with that of RecB and RecC ($R = 0.48$ for both) and negatively correlated with that of AddAB ($R < -0.26$; Figure 6B). This suggests that RecBC might play a role in spacer acquisition for type I-F CRISPR-Cas systems.

The presence of type II-A CRISPR-Cas systems is positively correlated with the presence of AddAB ($R > 0.16$; Figure 6B), and their functional co-dependance is confirmed by the *Staphylococcus aureus* type II-A CRISPR-Cas system, which requires AddAB for efficient spacer acquisition.[58] Similarly, spacer acquisition by the *Staphylococcus epidermidis* type III-A CRISPR-Cas system is also enhanced by AddAB,[59] in line with the positive correlation of the presence of AddA with type III-A CRISPR systems ($R = 0.09$; Figure 6B). When considering each phylum separately, the overall co-occurrences get stronger, and additional phyla-specific co-occurrences become apparent (Data S1A). For example, in Pseudomonadota, positive correlations between the presence of RecF and type I-B and I-F CRISPR-Cas systems and RecO with type I-F CRISPR-Cas systems exist, while in Bacillota, a negative correlation between the presence of AddB and type III-B CRISPR-Cas systems exists (Data S1A). Combined, these results reveal that there is no strict co-dependence of CRISPR-Cas subtypes on distinct DNA repair proteins, but they function in conjunction with specific preferences within phyla.

Despite RecBCD and AddAB having been implicated in generating small DNA guides for certain pAgos from the long-A pAgo clade,[62,63] a previous analysis suggests that RecBCD and AddAB are present in only 47% of genomes encoding catalytically active long-A pAgos.[63] In line with that observation, no moderate/strong correlations ($R > 0.10$) between the presence of any of the pAgo subtypes (including long A) and DNA repair proteins are observed across all phyla (Figure 6B; Data S1B). Also within phyla, no strong correlations (based on system presence in >10 genomes) are observed (Data S1B). Instead, a weak positive correlation between the presence of pAgos with RecJ, AddA, and AddB exists ($R = 0.09$, 0.09, and 0.08, respectively), and a weak negative correlation between the presence of pAgos with RecBC and AdnAB exists (all $R = -0.08$) (Figure 6B). This suggests that while (long-A) pAgos might be able to utilize the products of DNA repair proteins as guides,[62,63] they are functionally not strictly dependent on them.

Beyond these correlations, the analysis uncovers hitherto unreported (but mostly weak) correlations for the presence of DNA repair proteins and Wadjet, MazEF, dGTPases, GAPS2, Charlie_gp32, and more (Figure 6B; Data S1C). Wadjet is an SMC protein complex that senses DNA topology (small circular vs. linear/long circular) and a nuclease that cleaves upon complex stalling.[93,94] In line with previous observations that Wadjet is typically found in Actinomycetota,[91] its presence is positively correlated with the presence of AdnAB ($R \geq 0.30$) and negatively correlated with RecJ ($R = -0.25$; Figure 6B). The toxin-antitoxin system MazEF, which a.o. senses DNA damage,[95] is positively correlated with RecJ ($R = 0.18$) and negatively correlated with AdnAB ($R = -0.16$).

It is possible that their functional mechanisms are linked to the activity of DNA repair proteins. Furthermore, 44 out of 64 GAPS2 systems were found together with a dGTPase ($R = 0.44$; Data S1C), which suggests possible synergy between these systems. These and other correlations provide leads for further investigation into synergies between immune systems and DNA repair proteins (Figure 6B; Data S1C).

Discussion:

Bacteria encode a wide array of DNA repair proteins, but which DNA repair proteins co-occur and/or are mutually exclusive has remained largely unclear, possibly due to challenges in accurate classification. In this study, we present an enhanced method for the classification of DNA repair proteins through reverse search score classification from various phylogenetic groups (Figure 2). This has facilitated in-depth analysis of the taxonomic distribution (Figure 3), co-occurrence, and genomic clustering of DNA repair proteins (Figure 4) and their abundance in relation to genome size (Figure 5). Finally, co-occurrence analysis between DNA repair proteins and prokaryotic immune systems was performed (Figure 8).

By analyzing the abundance of DNA repair proteins across non-redundant genome databases, we show that RecBCD is less conserved than previously thought,[69,70,71] as it occurs only (and often sporadically) in 9 out of 21 of the studied bacterial phyla (Figure 5). Most other bacteria encode either AddAB (most common) or AdnAB (specific to Actinomycetota). Yet, bacteria from other clades, particularly bacteria from various Terrabacterial clades, do not encode any of these canonical DSB repair complexes. The small genome size of Mycoplasmatota (many intracellular symbionts[100]) and Aquificota (Figure S5) could explain the lack of these DSB repair complexes, as was described previously.[72] However, this does not explain the absence of DSB repair complexes in Cyanobacteriota and Chloroflexota (Figures 3 and S5).[101,102] Possibly, in these species, RecA self-loading[103] is sufficient to stimulate HR without auxiliary proteins, or possibly other proteins mediate DSB repair, for example RecQ/RecS and RecJ together with RecFOR.[36] We can also not rule out that certain bacteria contain alternative DNA repair proteins that facilitate DSB repair, for example more remote homologs of RecBCD/AddAB (akin to AdnAB in Actinomycetota) or non-related DNA repair proteins with analogous functionality.

Exploration of the co-occurrence of bacterial immune systems and DNA repair systems confirms earlier observed correlations (e.g., for CRISPR-Cas systems and RecBCD[71]; Data S1A) but also reveals numerous novel correlations (Figure 6B; Data S1), which suggests that these DNA repair proteins and immune systems might function in conjunction. While pAgo proteins might be guided by RecBCD/AddAB-generated DNA fragments, we found no strong correlations between long-A pAgos and RecBCD or AddAB (Figure 6B). This suggests that DNA-guided pAgos might also rely on other mechanisms, including chopping,[64,109,110] or other nucleases that degrade invader DNA. Of note, Cyanobacteriota lack RecBCD and AddAB, but many Cyanobacterial long-A pAgos are co-encoded with putative Cas4 family nucleases (part of the PD-(D/E)XK nuclease superfamily[111] also encompassing AddAB, RecBC, and AdnAB; Figure 1C).[112,113]

The presence of various other immune systems, including dGTPases, GAPS2, Wadjet, MazEF, and Charlie_gp32, is positively correlated with DNA repair proteins (Figure 6B). While it remains unknown whether any functional relevance underlies these correlations, these and other co-occurrences (e.g., those observed for CRISPR-Cas systems) are never strict. Therefore, in support of the notion that prokaryotic immune systems are generally extensively transferred between bacteria and archaea from distinct phylogenetic clades,[114,115] we conclude that immune systems never exclusively rely on specific DNA repair proteins but that, in certain species, the immune and DNA repair might function in conjunction.

Beyond DNA repair proteins being important for maintaining genome integrity and function as immune systems, mobile genetic elements exploit or inhibit DNA repair proteins for natural transformation or recombination.[116,117,118] As such, DNA repair proteins influence the spread of mobile genetic elements and horizontal gene transfer and facilitate genome diversification. Given that prokaryotic immune systems are regularly transferred by horizontal gene transfer,[114,115] the observed associations of immune systems with DNA repair proteins could also be the result of enhanced horizontal gene transfer in that host or limited horizontal gene transfer in others. Finally, DNA repair proteins have been repurposed for genome engineering techniques.[119,120,121] As such, understanding the distribution of recombinatorial DNA repair systems can improve our knowledge of gene dissemination and might contribute to enhancing genome engineering techniques.

Limitations of the study:

Our method accurately identifies commonly studied DNA repair proteins that initiate HR and can be extended to other DNA repair proteins for a more comprehensive view of the DNA repair landscape. However, our analysis is limited by the diversity of available whole-genome sequences in the RefSeq database. As a result, in our analyses, Pseudomonadota, Actinomycetota, and Bacillota are overrepresented. Analyses on curated databases with a set of genomes that are equally distributed could facilitate a fairer distribution analyses.

We would like to emphasize that functional redundancy between DNA repair proteins might exist; a specific immune system might function in conjunction with RecBCD in one bacterium but with AddAB in another. Furthermore, correlations involving epistatic groups (e.g., RecBC and AddAB) may not always imply functional (in)compatibility; alternatively, such correlations could result from the presence/absence of another protein with functional (in)compatibility.

Certain correlations observed might be caused by a skewed phyletic distribution. This is, for example, the case for various correlations involving AdnAB observed in Actinomycetota. This could mean that the presence of AdnAB and certain immune systems are correlated simply because they are limited to the same phylum. However, since DNA replication proteins, and especially immune systems, are often horizontally transferred,[79,80,114,115] these restricted correlations could imply a functional dependence.

Additionally, analyzing data at the phylum level increases the strength and significance of correlations between the presence of DNA repair proteins and immune systems, but it reduces the overall biological relevance of these correlations. These co-occurrences will not only depend on the specific genetic context (i.e., what other proteins are encoded), but also the ecological environment of the species should be considered (e.g., intracellular symbionts might be less exposed to invading DNA and/or less exposed to DNA-damaging agents). As such, the correlations discovered in our analysis provide a solid *in silico* basis that will require further experimental investigation to reveal the putative mechanisms underlying the observed correlations.

Self-monitoring of blood glucose (SMBG) (the "fingerstick" method using a glucose meter) and A1C testing are frequently used to monitor patients with diabetes. Such methods, although ubiquitous, do not completely address glycemic control. SMBG is relatively inexpensive and easily learned by patients. However, it provides glucose concentrations at a single point in time, with no information about the trend of the glucose level (i.e., whether glucose is increasing or decreasing). A1C provides information about a patient's average blood glucose control during the previous 3 months, but it fails to provide data regarding daily glucose excursions or time spent in the target glucose range.

In contrast, CGM provides trending information and data on the percentage of time spent in and out of the target range (whether in hypoglycemia or hyperglycemia), as well as meal and activity markers. Its use has been demonstrated to be effective in detecting and reducing hypoglycemia and improving glycemic control in patients with type 1 or type 2 diabetes (10–15).

Two types of CGM systems are available: professional CGM (P-CGM, also known as "masked" or "retrospective" CGM) and real-time CGM (RT-CGM). Both types of CGM systems measure interstitial glucose levels through a subcutaneous sensor that reports a value every 5 minutes, or 288 times per day. This article focuses on P-CGM because RT-CGM has rarely been used in patients with type 2 diabetes.

P-CGM typically involves monitoring for a 6- to 14-day period in which the patient wears the sensor while conducting normal daily activities. The patient is "masked" to the sensor glucose values while wearing the P-CGM device and is not privy to them until the stored data are downloaded and analyzed at a physician's office. The goal of P-CGM is to assess glycemic patterns and understand how they are influenced by diet, glucose-lowering medications, and physical activity. In contrast, RT-CGM devices notify the patient of glycemic highs and lows, which usually results in the patient taking some action. Thus, the advantage of P-CGM over RT-CGM is that the patient's behavior is not influenced by the continuous feedback of glucose results.

Therefore, the health care provider (HCP) can view results that have not been influenced by a patient's decisions in real-time, which can improve understanding of the various factors influencing the patient's glycemic control. This helps the HCP make appropriate therapeutic treatment recommendations, including changes in diet, activity, and medication. In addition, a strong educational effect occurs when the HCP shares the report with the patient that can enhance patient engagement and motivation. The combination of these factors leads to improved glucose control (16–18).

Commercially Available CGM Devices:

CGM technology generally uses a glucose oxidase enzyme that converts glucose to hydrogen peroxide, which reacts with platinum inside the sensor located in the interstitial fluid. This generates a signal that is converted via an algorithm to a glucose reading. The wearable sensor is typically slightly larger than a quarter. Patients also log meals, medications, and activities, either on paper or via a mobile app. In the United States, there are currently three major manufacturers of U.S. Food and Drug Administration (FDA)-approved P-CGM devices: Medtronic, Dexcom, and Abbott. The systems are briefly described in Table 1.

TABLE 1.

Comparison of P-CGM Systems by Manufacturer (7,8)

	Medtronic iPro2 P-CGM	**Dexcom G4 Platinum**	**Abbott FreeStyle Libre Pro**
Duration of use (days)	6	7	14
Insertion site	Abdomen	Abdomen	Upper arm
Number of components	2 (sensor and recorder)	3 (transmitter, sensor, and receiver)	2 (sensor and reader)
Minimum number of calibrations per day	2	2	0
Reading frequency (min)	5	5	15
Operational temperature (°F)	36–86	36–77	50–86

Medtronic:

The first P-CGM device was the MiniMed physician-use glucose monitoring system (CGMS Gold), approved by the FDA in 1999. Medtronic launched the HCP-owned iPro2 system in 2009 and received FDA approval for the 6-day Enlite sensor wear in 2016. Data from the iPro2 system are uploaded into an Internet-based software system (CareLink) that calculates sensor glucose values using transmitted signals and requires at least four fingerstick calibrations per day. The sensor is disposable, whereas the recorder can be reused.

Dexcom:

Dexcom G4 PLATINUM is a practiceowned P-CGM device. It displays glucose readings every 5 minutes for up to 7 days. It is a two-in-one P-CGM device designed so that it can either provide real-time feedback and insights that can be used to make therapeutic treatment adjustments by the patient or can be masked by installing additional software so that it operates in a way similar to the Medtronic iPro2 system. The sensor is disposable, whereas the transmitter and receiver can be reused. This system requires at least two calibrations per day.

The influence of the immune system: a threshold for healing:

The system is bi-stable between healing and decay:

Numerical simulations of the system with fixed parameters show that there is a split in outcomes between healthy healing (the steady state) and a decay of the lung epithelium with strongly elevated immune cell numbers (the steady state). The first is displayed in yellow in the top row of panels in Fig. 3. It shows a healthy healing process of strongly damaged epithelium, which lasts around 15–30 days and returns the epithelium back to its defined healthy cell density. The adaptive immune system, modeled by , in this case also returns back to the healthy healed state of . The bottom row of panels in Fig. 3 shows a completely different outcome of the healing process. In this case, the epithelial cell density drops to zero within around 50 days. The immune cells persist at strongly elevated levels. Both chemicals, and , are equally elevated.

FIGURE 9.

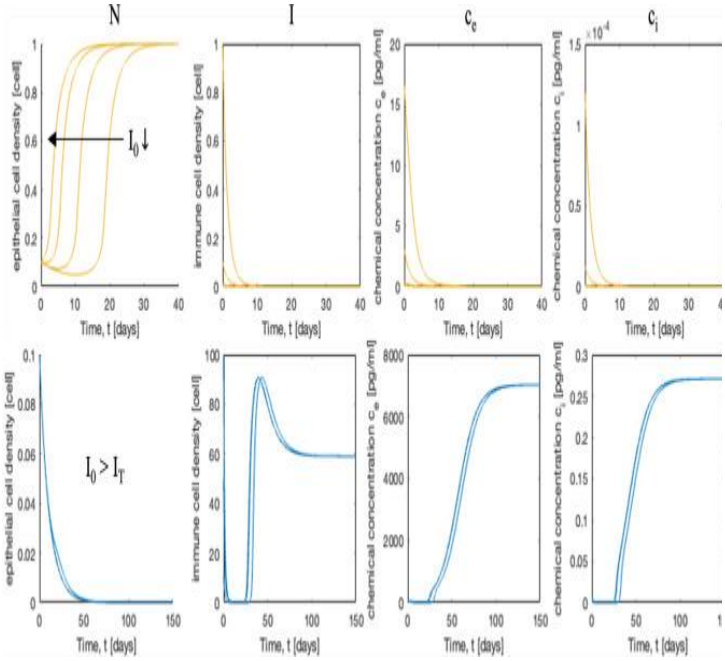

Fig. 9. Numerical simulation of the coupled system of ODEs. Plotted are the solution curves of all variables against time.

From left to right we show: epithelial cell density (healing/decay curves), immune cell density () curves, epithelial chemical concentration () curves [pg/ml] e.g. IL22, immune chemical concentration () curves [pg/ml] e.g. IL6. Damage is set at 90%, i.e. the initial epithelial cell density is . The value of the initial immune cell density is varied from 0.001 to . Interpretation of the value of the model immune cell density is discussed in Appendix B. The top row of graphs displays the simulation results of and the outcome is healthy healing, i.e. the system converges to the state . The bottom row of graphs shows the simulation results of , with an outcome of epithelial decay and strongly elevated immune levels, i.e. the system converges to the state . This indicates a threshold value of the immune response between and cells per unit volume, to allow for healing (yellow curves) instead of decay (blue curves). This threshold is also indicated in Fig. 5. The exact value of the threshold depends on the level of damage of the epithelium. Parameter values are fixed at (Crystal, 2014), , (Crystal, 2014), , (Kim et al., 1998), (Kim et al., 1998), (Zhang et al., 1997), , , (Chan et al., 1991), , , , , , , , . A detailed parameter estimation is given in Appendix A. The simulation is set-up using the MATLAB ODE-solver 'ode45', with time-steps and a relative and absolute tolerance of 10^{-13} and 10^{-20} respectively.

As can be seen from the two different outcomes of the top/bottom panels, there exists a threshold value of . As the threshold is passed, the healing outcome shifts from fully healing (yellow curves) to total decay of the epithelium (blue). This is not reversed or changed as we further increase
.

Definition of damage to the epithelium:

Damage to the epithelium is defined as the percent attenuation of the healed epithelial cell density and hence gives the initial condition for as
.

The healing of the lung is characterized by several stages, which indicate that proliferation of epithelial cells follows after the inflammation of the tissues. The phase of inflammation is not explicitly modeled by our system of ODEs. However, we implicitly include its effect through the initial immune cell density
. Fig. 9 shows the model solutions for different intensities of initial immune system responses, . Biologically, a larger corresponds to a stronger response of the immune system during the inflammation phase, which has left over a larger immune cell population density in the subsequent proliferation phase (the phase we model). Therefore, a strong inflammation response is captured by a high value of . For highly damaged epithelium (damage), we observe that the immune response is a critical component of the healing outcome (Fig. 9). If the value of
is too high (blue curves), the system converges to a steady state with zero epithelial cells per unit volume, which corresponds to a total decay of the lung epithelium. We briefly note here that this effect is not restricted to very high damage, as discussed in Section 3.2.

Strongly elevated equilibrium levels for chemicals and immune cells in the defective healing case:

In the blue epithelial cell density curves (high) we find almost identical decay profiles for the various values. Note here the different time-scales from 40 days (yellow) to 60 days (blue) until the epithelial cell population is in steady state. This effect is most apparent for the chemical concentrations (third and fourth panels) which increase from 10 days to 100 days until steady state is reached. We also observe strongly elevated equilibrium levels of both chemicals, known as a 'cytokine storm' in the literature, and a non-zero equilibrium immune cell density in the defective healing case (blue). In the healthy healing case, the epithelial chemical concentration returns to its defined equilibrium level of (i.e. 0.001 pg/ml), shown in the third yellow panel.

We have previously mentioned a link between prolonged immune cell influx during inflammation and a possible negative outcome of healing due to neutrophils damaging the ECM. Although these cells are not included in our model, we can nonetheless see this effect in the simulations of the decay outcome, which has an elevated initial density of immune cells (i.e. elevated immune cell density during inflammation). Furthermore, the immune cell density remains elevated at the steady state level in the case of the decay outcome. It could be interpreted that this elevated influx of immune cells also indicates an elevated influx of neutrophils which damage the ECM, therefore hindering healthy healing and supporting the decay outcome.

For the fastest healing speed of the lung epithelium, the immune system needs to be suppressed to the lowest possible level:

In the yellow epithelial cell density curves of Fig. 8 (low) we have several healing curves which are shifted relative to each other. The leftmost curve is for the lowest initial immune cell density and shifts to the right as is step-wise increased. This means that an increase in immune response corresponds directly to an increase in healing time, as shown in Fig. 9. The healing time is increased in a non-linear way, from a minimum of 8 days to a maximum of around 24 days at the threshold to decay. This means that for the fastest healing speed of the lung epithelium, the immune system should be suppressed to the lowest possible level. (We note that this is technically only true for , i.e. damage , which is most probably a biologically insignificant constraint.)

A comparison to clinical outcomes of lung injury (ARDS induced by COVID-19 infection) shows that the timescale of healing is approximately realistic. Patients admitted to the intensive care unit (ICU) recover within around 20 days from admission to discharge (Maggio et al., 2022). For the case study of a patient with a fatal case of COVID-19 induced ARDS, the approximate time spent in the ICU is also around 20 days, but admission was markedly at a later time-point of the infection and the disease had already progressed further (Deliwala et al., 2020). We therefore estimate that the time-frame of non-recovery, given by our simulations, of around 40–50 days is also approximately realistic.

A similar non-linear effect of increase in healing time is observed for a gradual increase in damage (from 10% to 99.99%), with fixed immune response, shown in Fig. 9.We further note that a case study of two brothers (Maggio et al., 2022) remarks on a strong link between clinical manifestations of disease severity (COVID-19 pneumonia), healing time (time spent in the ICU) and elevated cytokine levels (IL6). We observe this exact dynamic between healing time, damage levels and cytokine concentrations) in our model simulations, see Fig. 3. Measured levels of IL6 alone, in the outcome of healthy healing, vary between pg/ml in the two patients. Our simulation results predict much lower levels of the chemical (including IL6), which might be a consequence of the choice that our model variable contains both chemicals recruiting the immune system (such as IL6) and chemicals which inhibit it. It is therefore not possible to compare the numerical value of this variable to clinical measurements of IL6 directly.

As a reminder, we would like to investigate the influence of the immune system on the outcomes of the healing process of severe cases of lung injury.

FIGURE 10.

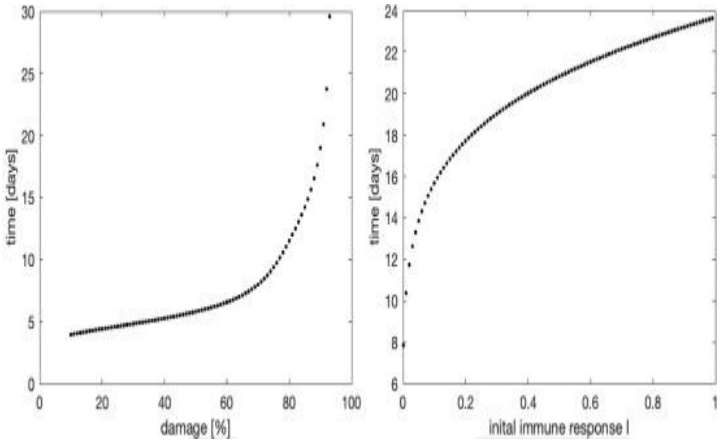

Fig. 10. The increased healing time (healing-lag) for the epithelial cell density, observed for increasing the initial immune response or damage. (Left) Varying initial damage from 11% up to 94%. The immune-response is fixed at

(30% of a normal immune response of 6 (Alberts et al., 2008) cells per unit volume). Shown is the time (in days) it takes for the epithelial cell density to reach 90% of the healed epithelial cell density . (Right) Damage is fixed at 90% and the initial immune response is varied from to . The results show a non-linear increase in healing time for both an increase in initial immune response and damage levels. The simulation is set-up using the MATLAB ODE-solver 'ode45', with time-steps and a relative and absolute tolerance of 10^{-13} and 10^{-20} respectively.

The existence of the separatrix gives a threshold value for the immune response to predict recovery instead of decay of the lung epithelium:

This split in outcomes can be explained when consulting the phase plane of the system, shown in Fig. 10. We see that the saddle point steady state creates a separation into two regions (yellow/blue) along its stable manifold (red), which acts as a separatrix. States in the phase plane are given by their biological coordinates , the initial immune response and damage levels of the epithelium. Solutions with initial conditions above the separatrix (in the yellow region) converge to the stable steady state and solutions with initial conditions below it (blue region) converge to the stable steady state . Hence, the split in outcomes is characterized by the existence of the separatrix. This implies that for a fixed given level of epithelial damage (i.e.), we have a threshold of initial immune response , which cannot be surpassed for the system to still converge to the healthy steady state. If the initial immune response is larger than this threshold , the system will converge to the decay state.

This can be visualized in the phase plane as a horizontal line at the given level .. The point at which the line slices through the separatrix gives the threshold of the immune cell density for healing vs decay. This is illustrated in Fig. 5 by the dashed lines and the black dot, giving the immune threshold for a fixed level of damage.

FIGURE 11.

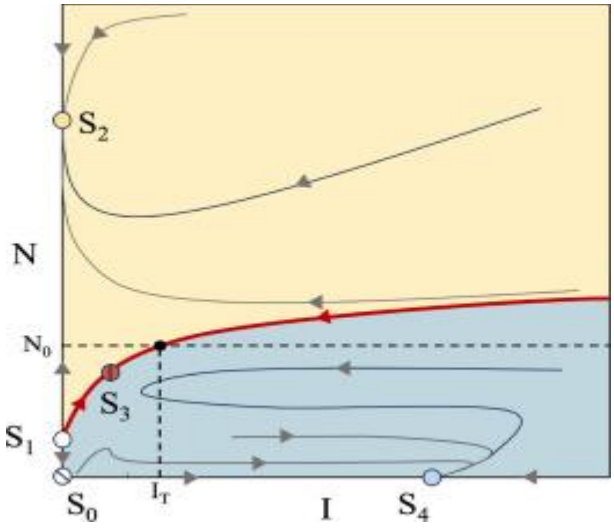

Fig. 11. A sketch of the phase plane where axes are not to accurate scale. The steady states are determined numerically by solving the locally linearized system of the two equations of the nullclines.

The saddle point:

and the stable state exist for any choice of parameters. The unstable state , saddle point and stable state are found for our fixed parameters as detailed in Fig. 11. The separatrix (red) between and to creates two outcomes for healing: convergence to epithelial decay or healthy healing , depending on damage and immune system levels, i.e. whether the system starts in the yellow or blue region. The black dot on the separatrix represents the immune threshold for the given level of epithelial cell density

Classification of outcomes based on parameter variation:

It is possible to influence the position and existence of the saddle point by a variation in parameters. This implies a change in the separatrix, which increases, decreases or completely eliminates the immune threshold for large enough parameter changes. In particular if the parameter is varied between its biologically realistic minimum and maximum values of zero and we obtain a classification of outcomes and immune thresholds. See Section 3.3 for the significance of . Qualitatively, decreasing the parameter causes an increase in the region of healing versus the region of decay in the phase plane. If is lower than a certain value the immune threshold and separatrix disappear and the region of healing is given by the entire biologically realistic set of initial conditions
. This outcome is most desirable medically. For a sketch of the phase plane in this case see Fig. 11 panel A.

FIGURE 12.

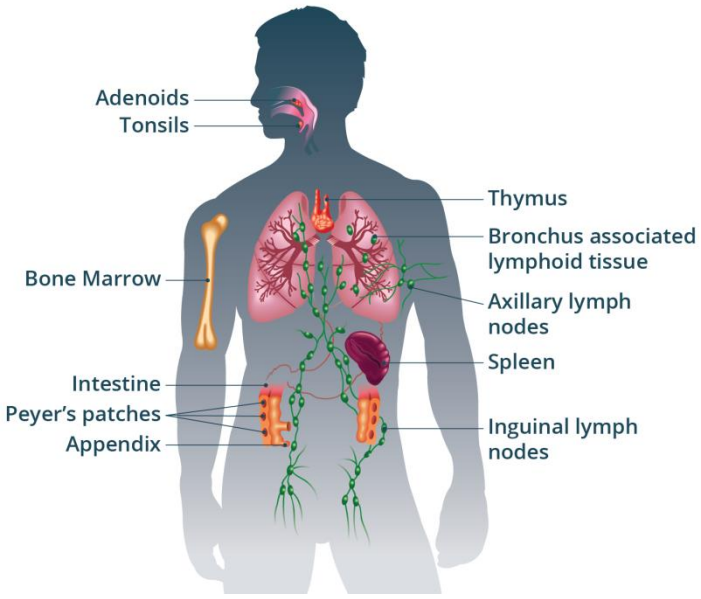

Definition of biological states of the system:

We will call the state of the system 'healed' if, from a given initial state , the system converges to the state . If the system converges to a different state with final cell density or , or , we will call it 'defective healing' and if , 'epithelial decay'. We can therefore classify the possible outcomes of the model as the parameter is varied. Our numerical simulations suggest three distinct healing outcomes. The classification of outcomes is obtained by linearizing the system to be able to conduct a stability analysis for all the steady states at varying values of . We show the three significant regions of
(X,Y and Z) in the bifurcation diagram of the system in Fig. 12 (see Table 12).

Region : is low enough such that no separatrix exists:

is characterized by the existence of only three steady states , and . In Fig. 6A, a representative phase plane for this range of is shown. The only attracting steady state is the healthy state . We note that if the epithelium is damaged in this case, the fastest healing will be given if the number of initial immune cells is zero. For highly damaged epithelium, the phase plane shows a hook-shaped trajectory which initially pulls the system towards the equilibrium, but then converges from an increased immune cell density to the healthy state. This corresponds biologically to an immune reaction, following damage to the epithelium, with full recovery to the healthy state. We further observe from the phase plane that if an individual starts with relatively low damage but elevated immune levels, the initial response will be a decrease in epithelial cell density while the immune cell density is reduced, followed by healing to the healthy state . This means that biologically, the region of represents a state of the lung which reacts to elevated immune levels with damage to the epithelium but is always able to recover without medical intervention, as expected realistically. Only if the damage has eliminated the epithelium completely does the system converge

to the defective state . The end of this region is marked by the appearance of the steady state. In Fig. 8, the bifurcation diagram of
, this is indicated by the neutral saddle bifurcation (red star).

Table 1. Definition of the three significant regions of and their biological states , which represent healthy or defective healing. In each region, the biological state are different, representing fundamentally different outcome possibilities to the healing process.

X The initial state
always converges to the **healed state**.
Fig. 10 A

Y The initial state
either converges to a **defective state** or to the **healed state** . Note: the defective state is very low in
.
Fig. 11 B,C

Z The initial state
either converges to the **healed state** or to the **decay state** .
Fig. 12 D,E,F

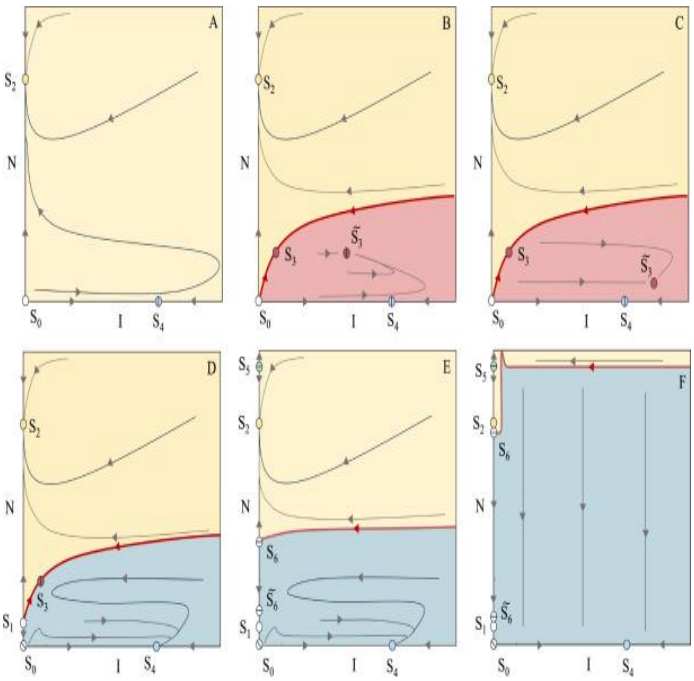

Fig. 11. Phase planes for distinct values of
. (A) , (B) (C) , (D) , (E) , (F) . Regions of convergence to respective stable states are colored yellow for , red for and blue for All other parameters are fixed as detailed in Fig. 3. The colored dots indicate stable nodes, the white dots indicate unstable nodes and the dots with a bar through them indicate saddle points.

The phase planes were obtained using MATLAB and sketched for illustrative purposes, where axes are not shown to scale.

FIGURE 14.

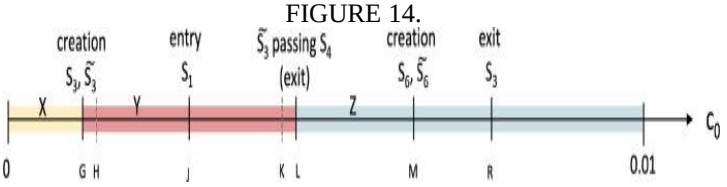

Fig. 12. Overview of the different regions of
, including significant changes to the steady states and phase plane of the system. Corresponding numerical values are approximated to the best of the authors abilities using MATLAB. The letters and indicate stability switches of the steady states. We denote by 'entry' and 'exit' of steady states the switch in one of the coordinates (or) to biologically realistic/unrealistic regimes (i.e. less than zero). The term 'creation' refers to a bifurcation event as shown in 12Fig. 11.

At , switches stability again from a stable node back to a saddle point, before shortly after, at , leaving the region of positive -coordinates. Simultaneous with the exit of , the stable node switches stability to a saddle point, marking the beginning of the blue region (), where is stable instead of a saddle node. This is significant as it means a change in the competing states of the bistable system from to . (In Fig. 6, panel shows a sketch between and .) The steady state stays a saddle point until, at , it becomes unstable and leaves the region of positive -coordinates. (In Fig. 14,)

The transition between regions
and is marked by the appearance of a pair of steady states and . (Illustrated by point
in Fig. 14.)

Region : **Introduction of the separatrix.** As :

is further increased, the two steady states denoted by and , in Fig. 14, Fig. 8, move apart (in both their - and -coordinates) until the lower of the two crosses the -axis and moves into biologically unrealistic regions. (This is the red branch point in 12Fig. 2). Note that this movement of in the -coordinate is very fast for small changes of , while stays relatively steady in its -coordinate, decreasing only very slowly (compare Fig. 11 and). The passing of through the -axis marks the end of the region , and the state simultaneously switches stability such that decay instead of healing defines the region below the separatrix. A sketch of the phase plane for values of within region is shown in Fig. 13 and , where the red region is defined by the separatrix with states below it converging to the stable (red) state . Biologically, this stable state represents very low levels of epithelial cell density, representing defective healing which might not be possible to be distinguished from epithelial decay, medically.

If initial conditions are above the red separatrix (yellow region), the system will converge to the healthy state as before. Biologically, this region of corresponds to disease states from

which individuals might not recover without medical intervention. We briefly note here that for any given level of damage to the epithelium (except), it is possible to rescue the healing process by decreasing the initial immune cell density sufficiently to cross the separatrix from the red region into the yellow region. This treatment suggestion will be addressed in more detail later (in Section 4.1). Biologically it could also be interpreted that this region of with convergence to represents some version of fibrosis (Warsinske et al., 2016).
The transition between regions and is marked by a stability switch of (from saddle point to stable node) and the disappearance of the into unrealistic regions (). Essentially, takes over the attracting characteristic of in the region below the separatrix. (Illustrated by point
in Fig. 7.)

***Region : The separatrix increases as it switches from* :**

The separatrix is the stable manifold of the state , which stays at a roughly constant level of . This steady state is a saddle point and slowly decreases its -coordinate (not shown in the bifurcation diagram in Fig. 8) until it passes the -axis (red branch point in Fig. 8). This branch point gives rise to two steady states denoted by and . (The corresponding value of is indicated in Fig. 7.) These two states are located on the -axis, and move apart as shown in the bifurcation diagram. This process is shown in the phase planes in Fig. 6 and . The separatrix is now given by the stable manifold of the
state.

As can be seen in Fig. 12 and , for initial states close to the separatrix with slightly elevated immune density levels, it is initially difficult to predict from the dynamic of and on which side of the separatrix the patient is currently located, i.e. whether healing or decay are predicted from the simulation. This is because in both cases, if close to the separatrix, the immune density levels will decrease initially with epithelial density levels staying relatively constant. This might be of medical interest as it describes a limitation of prediction of healing vs decay from the dynamics of the immune system. As is further increased, the state and the separatrix also increase in their -coordinates, hence making the region of convergence to the healed state in the phase plane smaller and smaller.

As a side note, the steady state appears much earlier than but is very low in and does not interfere with the separatrix. The significance of the state, existing even before this branching process and creating two more states, and , is that for extremely high levels of damage and zero immune cells the system now converges towards not , constituting a limitation on the treatment options, as discussed below. However, this restriction is most probably not significant from a medical perspective, as the -coordinate of is extremely low. This same implication is given by the state , which can take much larger values of , posing a realistic limitation to treatment.

Abbott:

Abbott recently received FDA approval for the Freestyle Libre Pro system. This system does not require fingerstick calibration, so patients do not need to be trained in performing SMBG for calibration. An HCP applies a small, round sensor on the back of the patient's upper arm. The sensor is held in place with a selfadhesive pad and remains on the back of the arm for up to 14 days.

P-CGM Reports

P-CGM reports facilitate an evidencebased dialog between the HCP and the patient. In recent years, there has been significant effort by manufacturers to make reports simple and easy to read, given PCPs' busy workdays. P-CGM reports typically show 1–14 days of glucose data. The reports are created in a PDF format, so they can be easily stored electronically or printed. Typical features of P-CGM reports include:

- **Daily overlay.** Provides an overlay of the sensor traces for each day on a single 24-hour graph that facilitates identification of trends or excursions that occur around the same time each day, including a summary of high and low glucose excursions and pie charts showing what percentage of each day the patient spent above, below, and within the target range.
- **Overlay by meal.** Provides an overlay of the sensor traces from each day of the study, broken down into meal and overnight periods, according to the meal recordings from the patient's logbook or smartphone app. The sensor traces for each day are overlaid so HCPs can look for trends at certain times related to meals or overnight periods. This report lines up glucose sensor traces before and after each meal and is especially useful if patients eat meals at varying times each day.
- **Daily summary.** Provides a summary of each full or partial 24-hour period of the study, including both the sensor trace and events such as meals, medications, and exercise.
- **Pattern snapshot report (Medtronic).** Provides a summary of daily glucose information and identifies up to three observed patterns based on rule-based algorithms. This report has three sections consisting of general statistics, observed patterns, and potential causes of these patterns.
- **Ambulatory glucose profile (AGP; Abbott).** A user-friendly chart providing HCPs a complete glycemic view of the patient's glucose trends for up to 14 days. The AGP helps identify when a patient is out of glucose range and provides hypoglycemia and hyperglycemia trends and patterns.

P-CGM reports may also include some key parameters, such as:

- **Average sensor glucose (SG).** Provides an average of all SG values during the current study.
- **Area under the curve (AUC).** Indicates the time spent in high and low excursions as above or below preset values.
- **Percentage high or low and time-in-range.** Excursion data indicating the frequency of high or low glucose levels.
- **Standard deviation (SD).** Measures variability in SG readings around the mean. The larger the SD, the greater the variability.
- **Estimated A1C (eA1C).** A value based on the A1C-Derived Average Glucose study (19) that defines a relationship between A1C and estimated average glucose.

References :

.Allen NA, Fain JA, Braun B, Chipkin SR. *Continuous glucose monitoring counseling improves physical activity behaviors of individuals with type 2 diabetes: a randomized clinical trial. Diabetes Res Clin Pract 2008;80:371–379* [DOI] [PMC free article] [PubMed] [Google Scholar]

American Diabetes Association America's diabetes challenge. Available from www.americasdiabeteschallenge.com. *Accessed 7 July 2017*

American Diabetes Association Cost of diabetes. Available from http://www.diabetes.org/advocacy/news-events/cost-of-diabetes.html. *Accessed 8 July 2017*

American Diabetes Association Glycemic targets. Sec. 6 in Standards of Medical Care in Diabetes—2017. Diabetes Care 2017;40(Suppl. 1):S48–S56 [DOI] [PMC free article] [PubMed] [Google Scholar]

American Diabetes Association Professional Practice Committee. 10. Cardiovascular Disease and Risk Management: Standards of Care in Diabetes—2024. Diabetes Care 2024, 47 (Suppl. S1), S179–S218. [Google Scholar] [CrossRef] [PubMed]

American Diabetes Association Professional Practice Committee. Classification and Diagnosis of Diabetes: Standards of Medical Care in Diabetes—2022. In Diabetes Care; American Diabetes Association Inc.: Arlington County, VA, USA, 2022; pp. S17–S38. [Google Scholar]

American Diabetes Association. Standards of Medical Care in Diabetes—2017 Abridged for Primary Care Providers. Clin. Diabetes 2017, 35, 5–26. [Google Scholar] [CrossRef]

Anderson, R.M.; Fitzgerald, J.T.; Gorenflo, D.W.; Oh, M.S. A Comparison of the Diabetes-related Attitudes of Health Care Professionals and Patients. Patient Educ. Couns. 1993, 21, 41–50. [Google Scholar] [CrossRef] [PubMed]

Aranda Parras, M.C.; Ballesterols Villar, J.; Crespo González, F.; del Burgo Fernández, J.L.; Domínguez Sánchez-Migallón, P.; Eliche Vilchez, J. Efectividad en el control de factores de riesgo cardiovascular en liabéticos tipo 2 de la provincia de ciudad real. Rev. Clin. Esp. 2005, 205, 218–222. [Google Scholar]

Aschner, P.; Gagliardino, J.J.; Ilkova, H.; Lavalle, F.; Ramachandran, A.; Mbanya, J.C.; Shestakova, M.; Chantelot, J.M.; Chan, J.C. Persistent poor glycaemic control in individuals with type 2 diabetes in developing countries: 12 years of real-world evidence of the International Diabetes Management Practices Study (IDMPS). Diabetologia 2020, 63, 711–721. [Google Scholar] [PubMed]

Beck RW, Tamborlane WV, Bergenstal RM, Miller KM, DuBose SN, Hall CA; T1D Exchange Clinic Network The T1D Exchange clinic registry. J Clin Endocrinol Metab 2012;97:4383–4389 [DOI] [PubMed] [Google Scholar]

Bertakis, K.D.; Franks, P.; Epstein, R.M. Patient-centered communication in primary care: Physician and patient gender and gender concordance. J. Womens Health 2009, 18, 539–545. [Google Scholar] [CrossRef]

Bertakis, K.D.; Helms, L.J.; Callahan, E.J.; Azari, R.; Robbins, J.A. The influence of gender on physician practice style. Med. Care 1995, 33, 407–416. [Google Scholar] [CrossRef]

Berthold, H.K.; Gouni-Berthold, I.; Bestehorn, K.P.; Böhm, M.; Krone, W. Physician gender is associated with the quality of type 2 diabetes care. J. Intern. Med. 2008, 264, 340–350. [Google Scholar] [CrossRef]

Bolíbar, B.; Fina Avilés, F.; Morros, R.; Del Mar Garcia-Gil, M.; Hermosilla, E.; Ramos, R.; Rosell, M.; Rodríguez, J.; Medina, M.; Calero, S.; et al. Base de datos SIDIAP: La historia clínica informatizada de Atención Primaria como fuente de información para la investigación epidemiológica. Med. Clin. 2012, 138, 617–621. [Google Scholar] [CrossRef]

Bouissiere, A.; Laperrouse, M.; Panjo, H.; Ringa, V.; Rigal, L.; Letrilliart, L. General practitioner gender and use of diagnostic procedures: A French cross-sectional study in training practices. BMJ Open 2022, 12, e054486. [Google Scholar] [CrossRef]

Campbell, J.L.; Ramsay, J.; Green, J. Practice size: Impact on consultation length, workload, and patient assessment of care. Br. J. Gen. Pract. 2001, 51, 644–650. [Google Scholar] [PubMed]

Centers for Disease Control and Prevention Ambulatory care use and physician office visits. 2017. Available from https://www.cdc.gov/nchs/fastats/physicianvisits.htm. *Accessed 20 June 2017*

Childs BP. The complexity of diabetes care. Diabetes Spectr 2005;18:130–131 [Google Scholar]

Coma, E.; Ferran, M.; Méndez, L.; Iglesias, B.; Fina, F.; Medina, M. Creation of a synthetic indicator of quality of care as a clinical management standard in primary care. SpringerPlus 2013, 2, 51. [Google Scholar] [CrossRef] [PubMed]

Davidson JA. The increasing role of primary care physicians in caring for patients with type 2 diabetes mellitus. Mayo Clin Proc 2010;85(Suppl. 12):S3–S4 [DOI] [PMC free article] [PubMed] [Google Scholar]

DCCT Research Group Diabetes Control and Complications Trial (DCCT): results of feasibility study. Diabetes Care 1987;10:1–19 [DOI] [PubMed] [Google Scholar]

de Oliveira AOT, Bartholomew K, Lavin-Tompkins J, Sperl-Hillen J. Use of continuous glucose monitoring as an educational tool in the primary care setting. Diabetes Spectr 2013;26:120–123 [Google Scholar]

Domínguez-Berjón, M.F.; Borrell, C.; Cano-Serral, G.; Esnaola, S.; Nolasco, A.; Pasarín, M.I.; Ramis, R.; Saurina, C.; Escolar-Pujolar, A. Constructing a deprivation index based on census data in large Spanish cities (the MEDEA project). Gac. Sanit. 2008, 22, 179–187. [Google Scholar] [PubMed]

ElSayed, N.A.; Aleppo, G.; Bannuru, R.R.; Beverly, E.A.; Bruemmer, D.; Collins, B.S.; Cusi, K.; Das, S.R.; Gibbons, C.H.; Giurini, J.M. Summary of Revisions: Standards of Care in Diabetes 2024. Diabetes Care 2024, 47 (Suppl. S1), S5–S10. [Google Scholar]

Fang, M.; Wang, D.; Coresh, J.; Selvin, E. Trends in Diabetes Treatment and Control in U.S. Adults, 1999–2018. N. Engl. J. Med. 2021, 384, 2219–2228. [Google Scholar] [CrossRef]

Fonseca VA, Grunberger G, Anhalt H, et al. ; Consensus Conference Writing Committee. Continuous glucose monitoring: a consensus conference of the American Association of Clinical Endocrinologists and American College of Endocrinology. Endocr Pract 2016;22:1008–1021 [DOI] [PubMed] [Google Scholar]

Franch-Nadal, J.; Mediavilla-Bravo, J.; Mata-Cases, M.; Mauricio, D.; Asensio, D.; Sarroca, J. Prevalence and control of type 2 diabetes mellitus among primary care physicians in Spain. PRISMA Study. Endocrinol. Diabetes Nutr. 2017, 64, 265–271. [Google Scholar] [CrossRef]

Garg SK, Voelmle MK, Beatson CR, et al. Use of continuous glucose monitoring in subjects with type 1 diabetes on multiple daily injections versus continuous subcutaneous insulin infusion therapy: a prospective 6-month study. Diabetes Care 2011;34:574–579 [DOI] [PMC free article] [PubMed] [Google Scholar]

Gehlaut RR, Dogbey GY, Schwartz FL, Marling CR, Shubrook JH. Hypoglycemia in type 2 diabetes: more common than you think: a continuous glucose monitoring study. J Diabetes Sci Technol 2015;9:999–1005 [DOI] [PMC free article] [PubMed] [Google Scholar]

Gencat. Indicadors de L'atenció Primària. Institut Català de la Salut. 2017. Available online: https://ics.gencat.cat/ca/assistencia/coneixement-assistencial/medicaments/indicadors-de-seguiment-de-la-prescripcio/indicadors-de-latencio-primaria/ (accessed on 16 October 2023).

Gencat. Memòria D'activitats 2017. Institut Català de la Salut. 2018. Available online: https://ics.gencat.cat/ca/lics/memories-dactivitat/memories-anteriors/memories-anteriors-de-lics/memoria-de-lics-2017 (accessed on 16 October 2023).

Generalitat de Catalunya. Atenció Primària 2017–2022: Central Resultats AQuAS 2023. Generalitat de Catalunya. 2023. Available online: https://aquas.gencat.cat/web/.content/minisite/aquas/publicacions/2023/atencio-primaria-2017-2022-central-resultats-aquas2023.pdf (accessed on 1 March 2024).

Generalitat de Catalunya. Guia Breu de Práctica Clínica Sobre la Diabetes Mellitus Tipus 2 [PDF]. Available online: https://ics.gencat.cat/web/.content/Documents/assistencia/gpc/Guia_breu_DM2.pdf (accessed on 1 August 2023).

Generalitat de Catalunya. Incentius per als Professionals D'atenció Primària a L'àmbit Rural. Generalitat de Catalunya [Updated 27 May 2019]. Available online: https://web.gencat.cat/es/actualitat/detall/Incentius-per-als-professionals-datencio-primaria-a-lambit-rural (accessed on 1 March 2024).

Gilabert-Perramon, A.; López-Calahorra, P.; Escoda-Geli, N.; Salvadó-Trias, C. Receta electrónica en Cataluña (Rec@t): Una herramienta de salud. Med. Clin. 2010, 134 (Suppl. S1), 49–55. [Google Scholar] [CrossRef] [PubMed]

González-Clemente, J.M. Nuevos fármacos para la diabetes mellitus tipo 2: Amigos o enemigos. Reflexiones sobre una nueva guía de armonización del tratamiento de la diabetes mellitus tipo 2. Av. Diabetol. 2014, 30, 91–94. [Google Scholar] [CrossRef]

Gravelle, H.; Liu, D.; Santos, R. How do clinical quality and patient satisfaction vary with provider size in primary care? Evidence from English general practice panel data. Soc. Sci. Med. 2022, 301, 114936. [Google Scholar] [CrossRef]

Helminen O, Pokka T, Tossavainen P, Ilonen J, Knip M, Veijola R. Continuous glucose monitoring and HbA1c in the evaluation of glucose metabolism in children at high risk for type 1 diabetes mellitus. Diabetes Res Clin Pract 2016;120:89–96 [DOI] [PubMed] [Google Scholar]

International Hypoglycaemia Study Group Minimizing hypoglycemia in diabetes. Diabetes Care 2015;38:1583–1591 [DOI] [PubMed] [Google Scholar]

International Diabetes Federation Diabetes Atlas. 7th ed. Brussels, Belgium, International Diabetes Federation, 2015 [Google Scholar]

Jadviscokova T, Fajkusova Z, Pallayova M, Luza J, Kuzmina G. Occurence of adverse events due to continuous glucose monitoring. Biomed Pap Med Fac Univ Palacky Olomouc Czech Repub 2007;151:263–266 [DOI] [PubMed] [Google Scholar]

JDRF Continuous Glucose Monitoring Study Group. Continuous glucose monitoring and intensive treatment of type 1 diabetes. N Engl J Med 2008;359:1464–1476 [DOI] [PubMed] [Google Scholar]

JDRF Continuous Glucose Monitoring Study Group. Effectiveness of continuous glucose monitoring in a clinical care environment: evidence from the Juvenile Diabetes Research Foundation Continuous Glucose Monitoring (JDRF-CGM) trial. Diabetes Care 2010;33:17–22 [DOI] [PMC free article] [PubMed] [Google Scholar]

Journath, G.; Hellénius, M.-L.; Manhem, K.; I Kjellgren, K.; Nilsson, P.M. Association of physician's sex with risk factor control in treated hypertensive patients from Swedish primary healthcare. J. Hypertens. 2008, 26, 2050–2056. [Google Scholar] [CrossRef] [PubMed]

Kazemian, P.; Shebl, F.M.; McCann, N.; Walensky, R.P.; Wexler, D.J. Evaluation of the Cascade of Diabetes Care in the United States, 2005–2016. JAMA Intern. Med. 2019, 179, 1376–1385. [Google Scholar] [CrossRef] [PubMed]

Khan, M.A.B.; Hashim, M.J.; King, J.K.; Govender, R.D.; *Mustafa, H.; Al Kaabi, J. Epidemiology of Type 2 Diabetes—Global Burden of Disease and Forecasted Trends. J. Epidemiol. Glob. Health 2020, 10, 107–111. [Google Scholar] [CrossRef]*

Kovács, N.; Varga, O.; Nagy, A.; Pálinkás, A.; Sipos, V.; Kőrösi, L.; Ádány, R.; Sándor, J. The impact of general practitioners' gender on process indicators in Hungarian primary healthcare: A nation-wide cross-sectional study. BMJ Open 2019, 9, e027296. [Google Scholar] [CrossRef] [PubMed]

Krass, I.; Schieback, P.; Dhippayom, T. Adherence to diabetes medication: A systematic review. Diabet. Med. 2015, 32, 725–737. [Google Scholar] [CrossRef]

Kushner, P.R.; Cavender, M.A.; Mende, C.W. Role of Primary Care Clinicians in the Management of Patients with Type 2 Diabetes and Cardiorenal Diseases. Clin. Diabetes 2022, 40, 401–412. [Google Scholar] [CrossRef]

Levengood, T.W.; Peng, Y.; Xiong, K.Z.; Song, Z.; Elder, R.; Ali, M.K.; Chin, M.H.; Allweiss, P.; Hunter, C.M.; Becenti, A. Team-Based Care to Improve Diabetes Management: A Community Guide Meta-analysis. Am. J. Prev. Med. 2019, 57, e17–e26. [Google Scholar] [CrossRef] [PubMed]

Lin, X.; Xu, Y.; Pan, X.; Xu, J.; Ding, Y.; Sun, X.; Song, X.; Ren, Y.; Shan, P.F. Global, regional, and national burden and trend of diabetes in 195 countries and territories: An analysis from 1990 to 2025. Sci. Rep. 2020, 10, 14790. [Google Scholar] [CrossRef]

Lu H, Holt JB, Cheng YJ, Zhang X, Onufrak S, Croft JB. Population-based geographic access to endocrinologists in the United States, 2012. BMC Health Serv Res 2015;15:541. [DOI] [PMC free article] [PubMed] [Google Scholar]

Mata-Cases, M.; Franch-Nadal, J.; Real, J.; Gratacòs, M.; López-Simarro, F.; Khunti, K.; Mauricio, D. Therapeutic inertia in patients treated with two or more antidiabetics in primary care: Factors predicting intensification of treatment. Diabetes Obes. Metab. 2018, 20, 103–112. [Google Scholar] [CrossRef]

Mata-Cases, M.; Mauricio, D.; Real, J.; Bolíbar, B.; Franch-Nadal, J. ¿Se registra y clasifica correctamente la diabetes mellitus en atención primaria? Estudio poblacional en Cataluña, España. Endocrinol. Nutr. 2016, 63, 440–448. [Google Scholar] [CrossRef]

Mata-Cases, M.; Roura-Olmeda, P.; Berengué-Iglesias, M.; Birulés-Pons, M.; Mundet-Tuduri, X.; Franch-Nadal, J.; Benito-Badorrey, B.; Cano-Pérez, J.F. Fifteen Years of Continuous Improvement of Quality Care of Type 2 Diabetes Mellitus in Primary Care in Catalonia, Spain. Int. J. Clin. Pract. 2012, 66, 289–298. [Google Scholar] [CrossRef] [PubMed]

Mata-Cases, M.; Vlacho, B.; Real, J.; Puig-Treserra, R.; Bundó, M.; Franch-Nadal, J.; Mauricio, D. Trends in the Degree of Control and Treatment of Cardiovascular Risk Factors in People with Type 2 Diabetes in a Primary Care Setting in Catalonia During 2007–2018. Front. Endocrinol. 2022, 12, 810757. [Google Scholar] [CrossRef]

Mohan V, Jain S, Kesavadev J, et al. Use of retrospective continuous glucose monitoring for optimizing management of type 2 diabetes in India. J Assoc Phys India 2016;64:16–21 [PubMed] [Google Scholar]

Mollo, A.; Vlacho, B.; Gratacos, M.; Mata-Cases, M.; Rubinat, E.; Berenguera Osso, A.; Cos, F.X.; Franch-Nadal, J.; Khunti, K.; Mauricio, D.; et al. A multicomponent health care intervention is associated with improved glycaemic control in subjects with poorly controlled type 2 diabetes compared with routine care: The INTEGRA study. Diabetes Obes. Metab. 2023, 25, 3549–3559. [Google Scholar] [CrossRef] [PubMed]

Nathan DM, Kuenen J, Borg R, Zheng H, Schoenfeld D, Heine RJ; A1c-Derived Average Glucose Study Group. Translating the A1C assay into estimated average glucose values. Diabetes Care 2008;31:1473–1478 [DOI] [PMC free article] [PubMed] [Google Scholar]

Nilsson, P.M.; Journath, G. Effective Consultation for Patients with Hypertension: Does the Physician's Gender Matter for Risk-Factor Contró? Women's Health 2008, 4, 433–434. [Google Scholar] [PubMed]

Nøkleby, K.; Berg, T.J.; Mdala, I.; Tran, A.T.; Bakke, Å.; Gjelsvik, B.; Claudi, T.; Cooper, J.G.; Løvaas, K.F.; Thue, G.; et al. Variation between general practitioners in type 2 diabetes processes of care. Prim. Care Diabetes 2021, 15, 495–501. [Google Scholar] [CrossRef]

Peters, S.A.E.; Muntner, P.; Woodward, M. Sex Differences in the Prevalence of, and Trends in, Cardiovascular Risk Factors, Treatment, and Control in the United States, 2001 to 2016. Circulation 2019, 139, 1025–1035. [Google Scholar] [CrossRef]

Peterson, T.A.; Fontil, V.; Koliwad, S.K.; Patel, A.; Butte, A.J. Quantifying Variation in Treatment Utilization for Type 2 Diabetes Across Five Major University of California Health Systems. Diabetes Care 2021, 44, 908–914. [Google Scholar] [CrossRef] [PubMed]

Peyrot, M.; Rubin, R.R.; Lauritzen, T.; Snoek, F.J.; Matthews, D.R.; Skovlund, S.E. Psychosocial problems and barriers to improved diabetes management: Results of the Cross-National Diabetes Attitudes, Wishes and Needs (DAWN) Study. Diabet. Med. 2004, 22, 1279–1385. [Google Scholar] [CrossRef] [PubMed]

Peytremann-Bridevaux, I.; Lauvergeon, S.; Mettler, D.; Burnand, B. Diabetes care: Opinions, needs and proposed solutions of Swiss patients and healthcare professionals: A qualitative study. Diabetes Res. Clin. Pract. 2012, 97, 242–250. [Google Scholar] [CrossRef] [PubMed]

Pinho-Gomes, A.C.; Peters, S.A.E.; Thomson, B.; Woodward, M. Sex differences in prevalence, treatment and control of cardiovascular risk factors in England. Heart 2021, 107, 462–467. [Google Scholar] [CrossRef]

Poolsup N, Suksomboon N, Kyaw AM. Systematic review and meta-analysis of the effectiveness of continuous glucose monitoring (CGM) on glucose control in diabetes. Diabetol Metab Syndr 2013;5:39. [DOI] [PMC free article] [PubMed] [Google Scholar]

Rawshani, A.; Rawshani, A.; Franzén, S.; Eliasson, B.; Svensson, A.-M.; Miftaraj, M.; McGuire, D.K.; Sattar, N.; Rosengren, A.; Gudbjörnsdottir, S. Mortality and Cardiovascular Disease in Type 1 and Type 2 Diabetes. N. Engl. J. Med. 2017, 376, 1407–1418. [Google Scholar] [CrossRef] [PubMed]

REDGDPS. Guía de Diabetes Tipo 2 Para Clínicos—Recomendaciones de la redGDPS. redGDPS. 2018. Available online: https://www.redgdps.org/guia-de-diabetes-tipo-2-para-clinicos/ (accessed on 17 January 2024).

Richard Grol, J.G. From best evidence to best practice: Effective implementation of change in patients' care. Lancet 2003, 362, 1225–1230. Available online: https://www.thelancet.com (accessed on 1 August 2023). [CrossRef]

Riordan, F.; McHugh, S.M.; O'donovan, C.; Mtshede, M.N.; Kearney, P.M. The Role of Physician and Practice Characteristics in the Quality of Diabetes Management in Primary Care: Systematic Review and Meta-analysis. J. Gen. Intern. Med. 2020, 35, 1836–1848. [Google Scholar] [CrossRef]

Sanz Tolosana, E.; Oliva Serrano, J. Local Perception of Access to Health Services in Rural Areas. 2021. Available online: https://pubmed.ncbi.nlm.nih.gov/34132244/ (accessed on 9 April 2023).

Sarría-Santamera, A.; Prado-Galbarro, J.; Ramallo-Farina, Y.; Quintana-Díaz, M.; Martínez-Virto, A.; Serrano-Aguilar, P. Use of emergency departments in rural and urban areas in Spain. Semergen 2014, 41, 63–69. [Google Scholar] [CrossRef]

Schmittdiel, J.A.; Traylor, A.; Uratsu, C.S.; Mangione, C.M.; Ferrara, A.; Subramanian, U. The association of patient-physician gender concordance with cardiovascular disease risk factor control and treatment in diabetes. J. Womens Health 2009, 18, 2065–2070. [Google Scholar] [CrossRef] [PubMed]

Scholes, S.; Fat, L.N.; Mindell, J.S. Trends in cardiovascular disease risk factors by BMI category among adults in England, 2003–2018. Obesity 2021, 29, 1347–1362. [Google Scholar] [CrossRef]

Seidu, S.; Cos, X.; Brunton, S.; Harris, S.B.; Jansson, S.P.O.; Mata-Cases, M.; Neijens, A.; Topsever, P.; Khunti, K. 2022 update to the position statement by Primary Care Diabetes Europe: A disease state approach to the pharmacological management of type 2 diabetes in primary care. Prim. Care Diabetes 2022, 16, 223–244. [Google Scholar] [CrossRef] [PubMed]

Sierra JA, Shah M, Gill MS, et al. Clinical and economic benefits of professional CGM among people with type 2 diabetes in the United States: analysis of claims and lab data. J Med Econ 2017. Epub ahead of print (DOI: 10.1080/13696998.2017.1390474) [DOI] [PubMed] [Google Scholar]

Simmons, D.; Lillis, S.; Swan, J.; Haar, J. Discordance in perceptions of barriers to diabetes care between patients and primary care and secondary care. Diabetes Care 2007, 30, 490–495. [Google Scholar] [CrossRef]

Tabenkin, H.; Eaton, C.B.; Roberts, M.B.; Parker, D.R.; McMurray, J.H.; Borkan, J. Differences in cardiovascular disease risk factor management in primary care by sex of physician and patient. Ann. Fam. Med. 2010, 8, 25–32. [Google Scholar] [CrossRef] [PubMed]

Tricco, A.C.; Ivers, N.M.; Grimshaw, J.M.; Moher, D.; Turner, L.; Galipeau, J.; Halperin, I.; Vachon, B.; Ramsay, T.; Manns, B.; et al. Effectiveness of quality improvement strategies on the management of diabetes: A systematic review and meta-analysis. Lancet 2012, 379, 2252–2261. [Google Scholar] [CrossRef] [PubMed]

Vigersky RA, Fish L, Hogan P, et al. The clinical endocrinology workforce: current status and future projections of supply and demand. J Clin Endocrinol Metab 2014;99:3112–3121 [DOI] [PubMed] [Google Scholar]

Vinagre, I.; Mata-Cases, M.; Hermosilla, E.; Morros, R.; Fina, F.; Rosell, M.; Castell, C.; Franch-Nadal, J.; Bolíbar, B.; Mauricio, D. Control of Glycemia and Cardiovascular Risk Factors in Patients with Type 2 Diabetes in Primary Care in Catalonia (Spain). Diabetes Care 2012, 35, 774–779. [Google Scholar] [CrossRef] [PubMed]

Vlacho, B.; Mata-Cases, M.; Mundet-Tudurí, X.; Vallès-Callol, J.-A.; Real, J.; Farre, M.; Cos, X.; Khunti, K.; Mauricio, D.; Franch-Nadal, J. Analysis of the Adherence and Safety of Second Oral Glucose-Lowering Therapy in Routine Practice from the Mediterranean Area: A Retrospective Cohort Study. Front. Endocrinol. 2021, 12, 708372. [Google Scholar] [CrossRef]

Yuguero, O.; Marsal, J.R.; Esquerda, M.; Galvan, L.; Soler-González, J. Cross-sectional study of the association between empathy and burnout and drug prescribing quality in primary care. Prim. Health Care Res. Dev. 2019, 20, e145. [Google Scholar] [CrossRef] [PubMed]